Technical Report

TR-06-41

Expansion due to the anaerobic corrosion of iron

N R Smart, A P Rance and P A H Fennell
Serco Assurance

December 2006

Svensk Kärnbränslehantering AB
Swedish Nuclear Fuel
and Waste Management Co
Box 5864
SE-102 40 Stockholm Sweden
Tel 08-459 84 00
+46 8 459 84 00
Fax 08-661 57 19
+46 8 661 57 19

Expansion due to the anaerobic corrosion of iron

N R Smart, A P Rance and P A H Fennell
Serco Assurance

December 2006

Executive Summary

The proposed design for a final repository for spent fuel and other long-lived residues in Sweden is based on the multi-barrier principle. The waste will be encapsulated in sealed cylindrical canisters, which will then be placed in vertical storage holes drilled in a series of caverns excavated from the granite bedrock at a depth of about 500 m and surrounded by compacted bentonite clay. The canister design is based on a thick cast inner container, designed to provide mechanical strength and to keep individual fuel bundles at a safe distance from one another, thereby minimising the risk of criticality. The container is fitted inside an inherently corrosion resistant copper overpack that is designed to provide containment over the long timescales required. As part of the safety case for the repository, one of the scenarios being addressed by SKB involves the early mechanical failure of the outer copper overpack, allowing water to enter the outer container and corrode the inner one. One consequence of this failure would be the long-term build up of corrosion product, which could induce stresses in the spent fuel canister.

A programme of experimental work was undertaken to investigate the effect of corrosion product formation on the generation of stresses in the outer copper container. This report describes the construction of an apparatus to directly measure the expansion caused by the anaerobic corrosion of ferrous material in a simulated repository environment whilst under representative compressive loads. This apparatus, known as the ‘stress cell’, consisted of a stack of interleaved carbon steel and copper discs that was subjected to a compressive load simulating the loads expected in a repository and immersed in simulated anoxic groundwater at 69°C. The stack was mounted in a rigid frame and a system of levers was used to amplify any expansion caused by corrosion; the expansion of the stack was measured using sensitive displacement transducers.

Initially, three cells were set up: two contained alternate carbon steel and copper discs, and the third, a control cell, consisted of alternate stainless steel and copper discs. A slight contraction of the control cell was observed but no expansion was measured in the carbon steel-copper cells. Analytical measurements showed that the corrosion products were magnetite and hydrogen, indicating that anaerobic corrosion was occurring. In a second series of experiments, one experiment was carried out in which carbon steel was replaced with cast iron and in a further experiment air was allowed to enter the test chamber. No expansion was detected in either of these additional experiments. However, expansion was detected when a separate stack of copper and steel washers was corroded in ambient atmospheric conditions under very small compressive loads, and subjected to a wet-dry cycle, demonstrating that the experimental technique was capable of detecting corrosion-induced expansion if it were occurring.

In parallel with the stress cell experiments, coupons of mild steel and cast iron were corroded in anoxic, artificial groundwater at 50°C and 80°C for several months. The coupons were examined using atomic force microscopy (AFM) to determine the mechanical properties and the structure of the corrosion product films, and X-ray photoelectron spectroscopy (XPS) to identify the chemical composition of the film. The report presents Young’s modulus, thickness and hardness data for the oxides, which were much more compliant than the magnetite films formed at high temperatures, probably because of their high water content. The report considers the application of the results to assessing the performance of the SKB canister in a repository situation.

Contents

1 Introduction

Nuclear reactors produce about 50% of all the electricity used in Sweden. By 2010 the current nuclear programme will have produced approximately 8,000 metric tons of spent nuclear fuel. After 30 to 40 years of storage in the intermediate storage facility, Clab, the fuel will be prepared for placement in a waste repository. The proposed design for a final repository for spent fuel and other long-lived residues in Sweden is based on the multi-barrier principle. The waste will be encapsulated in sealed corrosion resistant cylindrical canisters, which will then be placed in storage holes drilled in a series of caverns excavated from the granite bedrock at a depth of about 400–700 m, and surrounded by compacted bentonite clay. Once full, the facility will be backfilled and sealed with a mixture of bentonite and sand. The groundwater in granitic rock in Sweden is oxygen-free and reducing below a depth of 100 m to 200 m. The redox potential below this depth ranges between –200 and –300 mV on the hydrogen scale and the water has a pH ranging from neutral to mildly alkaline /1, 2/.

Resistance to corrosion can be achieved in several ways. SKB has decided to approach the long-term corrosion problem by choosing a container material that is as close as possible to being immune to corrosion under the expected repository conditions. Copper has a wide stability range in oxygen-free water /3/ and anoxic (i.e. oxygen-free) conditions are expected during most of the repository lifetime. Pure copper does not have sufficient mechanical strength to withstand the external overpressure of about 14 MPa that the canister will experience at the disposal level in the repository. This pressure is due to a combination of a hydraulic water pressure of 7 MPa, corresponding to a depth of 700 m, and a bentonite swelling pressure of 7 MPa. A cast iron or carbon steel insert in the 50 mm thick copper container is, therefore, used to give the waste package sufficient mechanical strength, as shown in Figure 1-1. The insert will also keep individual fuel elements at a safe distance from one another, thereby minimising the risk of criticality.

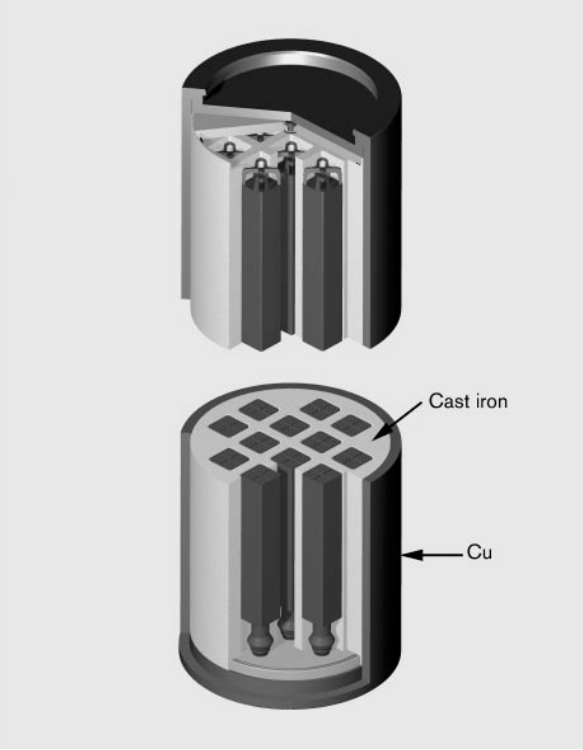

Figure 1-1. *Schematic diagram of SKB container design.*

As part of the safety case for the repository, one of the scenarios being addressed by SKB involves the possibility of early failure of the outer copper overpack, for example due to an undetected defect, which would allow groundwater to enter the outer container and corrode the inner one. The consequences of this failure would include:

- the long-term build up of solid corrosion product in the annulus between the inner and outer containers, which could induce stresses in the spent fuel canister because the volume of iron oxides are larger than the volume of the original metal (i.e. the Pilling-Bedworth ratio is > 1).
- anaerobic corrosion of the inner container, which would generate hydrogen that could disrupt the backfill in the repository or lead to the transport of radioactive gases.

The work described in the present report concentrates on investigating the first effect; the second, the rate of generation of hydrogen due to anaerobic corrosion, has been investigated previously /4–8/. If the outer copper container were to be breached, the inner steel container would start to corrode anaerobically and produce a layer of corrosion product whose volume would be greater than that of the original steel. Although the rate of formation of the corrosion product would be very low (long-term corrosion rates of the order of ~0.1 μm/yr have been measured), corrosion product could eventually fill the narrow annulus between the inner and outer containers and exert a load on both. The possible effect of corrosion product formation on the integrity of the container has been modelled using finite element techniques /9/. This work had to make assumptions about the mechanical properties of the corrosion product because no data were available for the corrosion products formed on iron at low temperatures under anoxic conditions.

The problem of damage caused by the formation and expansion of corrosion product in confined spaces has arisen in other contexts, particularly that of denting in steam generators on nuclear power stations, where corrosion product formed in the crevices between steel support plates and Inconel steam tubes, led to the collapse, and in some cases cracking, of the tubes as a result of the pressure generated by the corrosion product /10/.

Two approaches were taken during the current investigation. In the first, an apparatus was constructed to directly measure the expansion caused by the anaerobic corrosion of carbon steel and cast iron in a simulated SKB repository environment whilst under representative compressive loads. This apparatus was known as the ‘stress cell’. It consisted of a stack of alternate ferrous and copper washers that were corroded anaerobically in artificial groundwater. Changes in the height of the stack were monitored using a displacement transducer. The aim was to compare the results obtained from the experimental investigations with the results of the previous modelling exercise /9/. If agreement was found between the model and experiment the model would be validated and the degree of confidence for SKB and the Swedish regulatory authorities would be increased. Conversely, if agreement was not found the model could be modified accordingly.

A similar experimental approach, involving the use of a stack of metal discs to measure corrosion-induced expansion rates and hence corrosion rates, was employed previously by workers at CERL (Central Electricity Research Laboratories, U.K.) to obtain a continuous real-time value for the aerobic corrosion rate of steel under atmospheric conditions /11–13/. The technique was branded the ‘Environmental Corrosion Monitor’ (ECM). In these measurements the expansion of a 100-washer stack was measured using a linear voltage displacement transducer (LVDT) placed at the top of the stack, giving a sensitivity of ±0.01 μm per surface. The technique was used to obtain detailed measurements of the atmospheric corrosion rate, which were then correlated with information about the prevailing atmospheric conditions (e.g. sulphur dioxide concentration, relative humidity, temperature, time of wetness). The technique had a high sensitivity and gave a reproducible, uniform response because of the large number of specimens used. The technique was also applied to a number of other expansive corrosion issues, including study of the corrosion of concrete reinforcement bars, where alternate cement and steel discs were used in the test stack, and failures of insulators on electricity transmission lines caused by expansive corrosion in crevices /12/. The technique was also used to study galvanic interactions,

for example at aluminium-steel interfaces in electricity transmission lines that can be exposed to the atmosphere when protective coatings fail /12/. Good correlation was found between the ECM and weight loss measurements /13/, but the advantage of the ECM was that it gave a continuous measurements of corrosion, rather than the single integrated measurement provided by weight loss tests.

In the second approach to the problem, and in parallel with the stress cell experiments, the mechanical properties of the oxides formed during anaerobic corrosion of carbon steel and cast iron were investigated by corroding a set of coupons in two types of artificial groundwater at 50°C and 80°C for several months and then analysing the resulting solid corrosion products using atomic force microscopy (AFM).

This is the final report on the studies of anaerobic corrosion-induced expansion and the mechanical properties of iron oxides formed under anoxic conditions. It follows the publication of two conference papers on the early results from the programme /14, 15/. The report presents the experimental details of the measurements and discusses the results in the context of the probable canister performance in the planned Swedish geological repository.

2 Experimental

2.1 Stress cell apparatus

2.1.1 Overall design of experiment

The aim of the stress cell experiments was to set up a stack of copper and carbon steel or cast iron discs under mechanical conditions which simulated those expected in the SKB repository, whilst immersed in anoxic artificial groundwater, and to measure any expansion caused by corrosion of the discs. As the anaerobic corrosion rate of the ferrous material was expected to be very low, the increase in volume due to the corrosion of a single specimen over a reasonable period of exposure would be too small to be measured accurately by any instrumentation that would be compatible with immersion in simulated groundwater. It was therefore necessary to devise a method of amplifying any effects of corrosion product formation so that they could be measured more accurately. The method adopted was to set up a stack of one hundred carbon steel discs separated by copper discs and to measure the total expansion of the stack of discs. This design provided 200 copper-steel interfaces at which corrosion could take place. In addition, the use of alternating steel and copper discs simulated the combination of materials that would occur if the surfaces of the inner and outer containers of the SKB canister were to come into contact and ensured that the experiment simulated reality as far as was practicably possible. The expansion of the column was amplified further using a system of levers and the total movement was measured using a sensitive linear displacement voltage transducer (LVDT).

2.1.2 Design of stress cell apparatus

A schematic diagram of the stress cell is shown in Figure 2-1 and a key to the components is given in Table 2-1. Photographs of the assembled apparatus are shown in Figure 2-2 to Figure 2-5. The apparatus consisted of a stack of discs, nominally 251.5 mm high, which was mounted in a rigid, 6082T6 aluminium alloy frame. Any expansion of the stack would have caused rotation of the pivoted mount at the top of the stack and the movement would then have been transmitted to the first lever, which would have been elevated. The amplified displacement at the end of the first lever arm was measured using displacement transducers mounted in the frame.

The system of levers gave an amplification factor of 15.9 for the total expansion of the stack as measured at the point where the LVDT was located. High precision bearings were used and moving parts were lubricated. The amplification of any changes in the stack height, and the fact that two hundred corroding interfaces were present in the cell, represents a total magnification factor of 3,200 times relative to the expansion at a single corroding steel face. The theoretical detection limit for a change in specimen thickness was ~0.001 μm, compared to an expected initial corrosion rate of > 10 μm yr^{-1} /8/.

The lever arms were also used to transmit a compressive load to the stack of specimens, by placing lead shot in a holder at the end of a second lever arm. The applied load on the stack was monitored by means of load cells mounted directly in line with the specimen stack.

2.1.3 Specimen design

The carbon steel disc specimens had a thickness of 1 mm and a diameter of 38 mm. They were separated by 1.5 mm thick copper discs with the same diameter as the carbon steel. In a second set of experiments cast iron discs were used instead of carbon steel. The cast iron discs were thicker (3 mm) and so a smaller number was used. A central 10 mm diameter hole was machined in each specimen and a loose-fitting copper rod was inserted through the stack to provide stability.

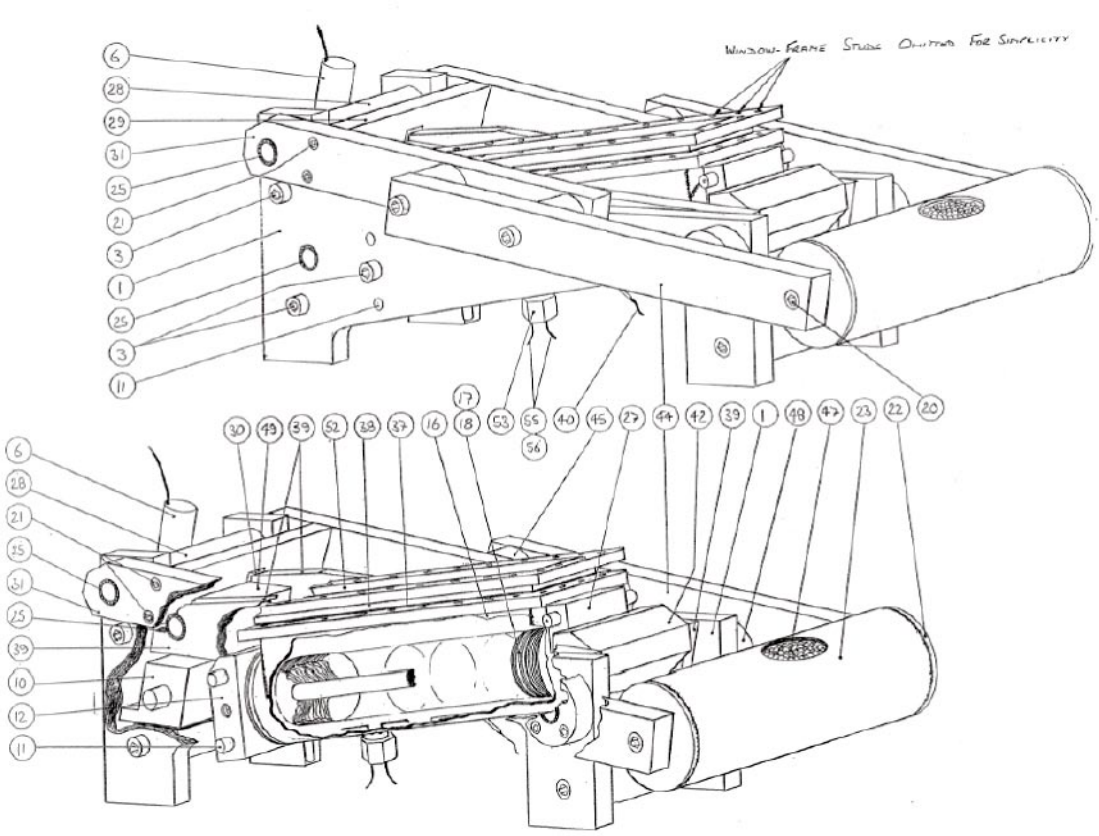

Figure 2-1. *Schematic diagram of stress cell apparatus (see Table 2-1 for key to components).*

Table 2-1. Key to Figure 2-1, showing main components of stress cell.

Component number	Identity	Component number	Identity
1	Side frame	29	Cross beam
3	M12 screw	30	Ball bearing
6	LVDT	31	Pin
10	Bearing housing block	37	Sealing gasket
11	Dowel	38	Viewing window
12	Lower support block	39	Primary loading side lever
16	Environmental chamber	40	Platinum resistance thermometer
17	Copper specimen	42	Upper test section support block
18	Iron specimen	44	Mass loading side arm
20	M12 Screw	45	Spacer bush
21	Spacer ring	47	Lead shot
22	Flange	48	Bearing housing block
23	Container for lead shot	49	Transducer support block
25	Needle bearing	52	Window clamp frame
27	Load cell	53	Gland nut
28	Dowel sleeve	55	Carbon steel wire
		56	Silver chloride reference electrode

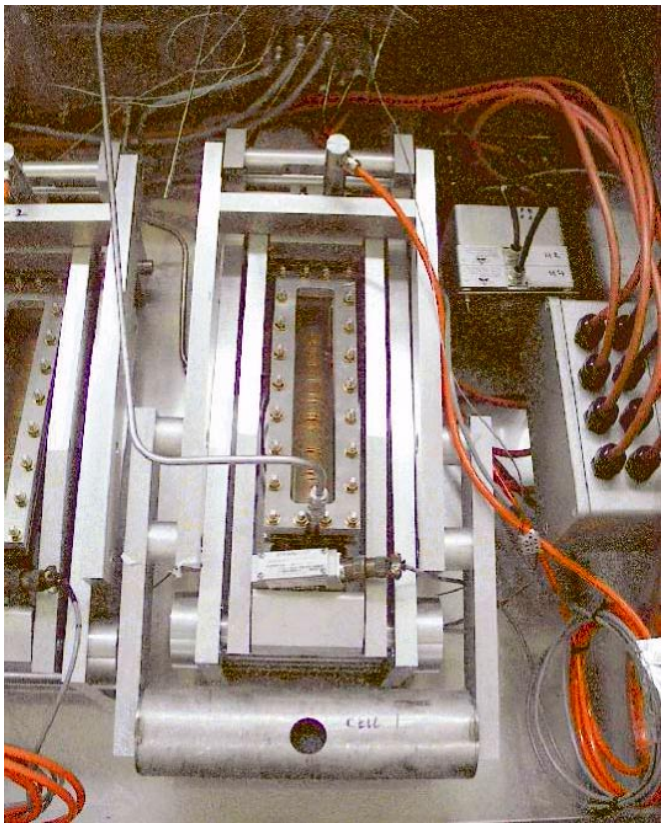

Figure 2-2. *Photograph of assembled apparatus.*

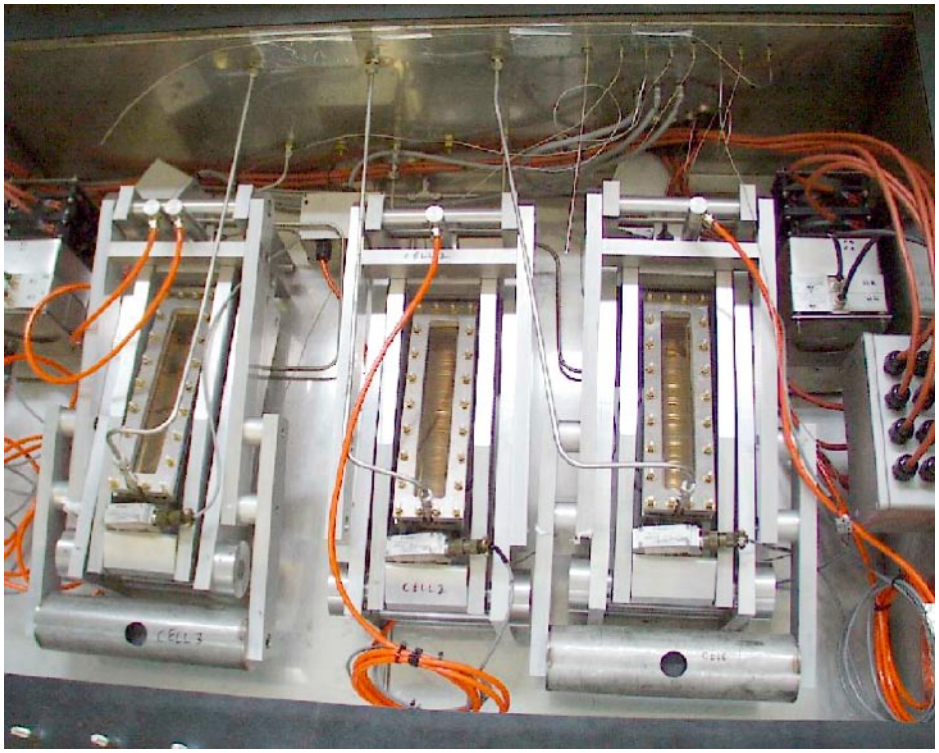

Figure 2-3. *The complete stress cell apparatus.*

Figure 2-4. *Three stress cells inside the environmental chamber, with the fluid reservoir in the background.*

Figure 2-5. *Control panel, datalogging system and manometers for stress cells.*

To ensure entry of water to the interface between the test specimens and to allow a free exit path for any gas produced during the corrosion process, the faces of the copper discs were impressed with a matrix of shallow concentric rings and radial lines. In addition, the surfaces of the copper discs were roughened by glass bead peening to provide a peak-to-peak height comparable in size to the thickness of the oxide expected on the surface of the corroding steel. Small-scale glass bead peening trials were carried out to establish the most suitable technique for roughening the surface. The roughness of bead-peened copper discs were measured using a surface profilometer (Dektak) and the roughness value, R_a, was chosen to be ~0.5 μm.

2.1.4 Environmental control and monitoring

The environment around the stack of discs was contained in a cylindrical stainless steel vessel that was sealed with a sliding O-ring system. The O-rings were mounted in carbon steel end caps that were located at each end of the stack. The stainless steel vessel was electrically insulated from the test stack by the O-rings and plastic inserts. The central supporting rod was located in a blind hole in each end cap. All the wetted metallic parts that were in electrical contact with the test specimens were made from mild steel or copper only, in order to prevent any extraneous galvanic effects. A transparent polysulphone viewing window was incorporated in the stainless steel vessel, using a flange and butyl rubber gasket arrangement, to allow visual inspection of the corroding specimens. Three complete cells were manufactured.

Stainless steel inlet and outlet pipes were provided to each test cell, (i) to enable the test solution to be drawn in to the test chambers, (ii) to enable a mild vacuum to be applied to the test cell to ensure wetting of the specimen surfaces when the test solution was drawn in, and (iii) to allow gas produced by anaerobic corrosion to escape. A reservoir containing the test solution was attached to the cell inlets and a nitrogen purge system was incorporated into it to enable the test solution to be deaerated prior to entry into the test cells. A manometer system, similar to those used for anaerobic corrosion gas cell measurements /6/, was attached to the outlets from each of the three test cells to enable changes in gas pressure to be detected. The size of the manometer was designed on the basis of the amount of hydrogen expected, based on previous experimental data (e.g. /4/). The manometer was arranged so that leakage of the external atmosphere into the test cell was prevented. The test stack was inclined at an angle of ~10° to the horizontal to encourage any gas produced by corrosion to escape through the outlet pipe located at the top end of the environmental vessel.

All three rigs were mounted inside a separate environmental cabinet, which was fabricated from stainless steel. The lid of the environmental chamber consisted of a pane of glass, which was sealed to the box using a butyl rubber gasket and a bolted clamping plate. The box was purged slowly with nitrogen, as a precaution to ensure that anoxic conditions were maintained within the test cells. The gas in the test chamber was heated and circulated using small electric fans attached to heaters. Electrical connections to the test rigs were made via hermetically sealed panel-mounting connections. The environmental chamber was mounted on vibration resistant feet. Two ‘ballast’ heaters were controlled manually by a variable transformer to raise the temperature to close to the required value and two ‘top-up’ heaters were used under the control of a Eurotherm controller to control the temperature to the correct value. This arrangement was used to ensure that if the controller failed for any reason the temperature would not fall to ambient. There were two permanently running circulation fans, with two backup fans that were designed to switch in automatically in case of failure. The motors from the fan heaters also provided a heat input into the test chamber.

Each test cell contained a carbon steel wire and a silver-silver chloride reference electrode. The corrosion potential of the carbon steel was measured to determine whether anaerobic corrosion was occurring. The oxygen concentration was not measured directly but it would be expected that any residual oxygen that was present at the start of the experiments would have been rapidly ‘gettered’ from the test chamber by the walls of the test cells and the corrosion specimens.

Platinum resistance thermometers were used to monitor and control the temperature of the gas in the environmental cabinet and chromel-alumel thermocouples were inserted into pockets in each of the three test cells to measure the temperature of the test solutions.

2.1.5 Electrical equipment

The following electrical equipment was provided:

- Temperature resistant LVDTs to monitor the change in the height of the specimen stack.
- Load cells, to monitor the load on the test stack.
- Panel meter displays for the load cells and displacement transducers.
- Heating and temperature control of the test cabinet.
- A wall-mounted box to contain the electrical monitoring and control equipment (Control Techniques), Figure 2-5.
- A PC-based datalogging system for displacement, load and temperature.

2.1.6 Materials

The compositions of the copper (ASTM C101 OFE copper), carbon steel (BS EN 10130:1991 Fe PO1 CR4) and cast iron (BS2789 Grade 420/12) used for the test specimens are given in Table 2-2. The carbon steel and copper discs were stamped out of sheet material. The stamping process resulted in slight curvature of the steel test coupons, but this was removed by flattening the specimens using a hand press. The cast iron discs were supplied by European Corrosion Supplies Ltd. Prior to use the surfaces of the carbon steel and cast iron were prepared by pickling them to remove air-formed oxides using the same procedure as that used for preparing samples for gas generation rate experiments /6/. This involved immersion in 10% HCl for five minutes, followed by washing in distilled water and ethanol. The specimens were stored in a nitrogen-purged glove box prior to fitting in the test rigs.

The copper was annealed (425°C for 1 hour in nitrogen) before the flow channels and surface roughening treatments were applied.

Artificial ‘bentonite-equilibrated groundwater’ was used as the test solution in the stress cell experiments. It was prepared using distilled water to which 31.56 g/litre sodium chloride and 1.06 g/litre sodium carbonate were added. The pH of freshly prepared solution was ~10.4.

2.1.7 Experimental procedure

Before the experiments were started, trials were carried out to test the mechanical linkages and to calibrate the LVDTs by applying a small, known mechanical displacement to the stack using a fine screw threaded device. The operation of the ancillary equipment for operating the test cells (e.g. preparing the test solutions, filling the test chambers and heating the solutions) was also tested. The procedure for setting up and running the experiments was as follows:

1. Prepared test specimens by cleaning and pickling.
2. Assembled the components of the test cells in the open atmosphere.

Table 2-2. Composition of materials used for test specimens in stress cell experiments (wt%).

	Fe	Cu	C	Mn	Si	P	S	Pb	Al	O2
carbon steel	rem		0.035	0.18	0.011	0.011	0.012		0.046	
copper		99.996				0.00005	<0.0005	0.0001		0.0003
cast iron	rem		3.65		2.29	<0.005	<0.005			

3. Placed test assemblies in test chamber and purged with nitrogen to protect pickled ferrous samples.
4. Connected transducer system for measuring expansion of specimen stack.
5. Compressed specimen stack by filling the lead shot containers to give the required loads. Allowed settling and primary creep to occur.
6. Deaerated reservoir of test solution by purging with high purity nitrogen for 48 hours.
7. Evacuated the pipework and the test cells and backfilled with nitrogen several times.
8. Evacuated the test cell then partially backfilled with nitrogen to leave a partial vacuum in the test cell; this ensured that liquid penetrated the interstices between the specimens. Released the solution from the reservoir and allowed it to fill the test cells under gravity.
9. Increased temperature slowly to 69°C, while purging the test cabinet with high purity nitrogen. This temperature was chosen to ensure that the pressure generated by heating the gas in the test chamber was not greater than the hydraulic head in the gas manometer.
10. Monitored load, displacement, temperature, height of liquid in the manometer columns and electrochemical potential of carbon steel electrodes.
11. At the end of the experiments dismantled cells and examined the specimens to determine the distribution and composition of corrosion product.

2.1.8 Test programme

In the first set of experiments the following three test cells in the rig were set up: in two of the cells, stacks of copper and carbon steel discs were used. In one experiment the applied compressive load at the top of the specimen stack was 10 MPa. The second cell was operated at a lower load (~1 MPa), to determine whether the applied load had any effect on the amount of expansion caused by corrosion product formation. The third cell was a control test at a compressive load of 10 MPa that used stainless steel discs rather than carbon steel, to ensure that any expansion measured in the other two experiments was due to corrosion and not some other unforeseen effects.

In a second series of experiments, stacks were set up with (i) cast iron specimens, rather than carbon steel, in artificial groundwater, and (ii) with carbon steel in aerated demineralised water, under a load of approximately 1 MPa. The experiments with cast iron were performed because separate corrosion tests (see Section 2.3.1) suggested that cast iron produces a thicker more voluminous corrosion product than carbon steel. The experiments under aerated conditions were designed to test the behaviour of the apparatus when rapid corrosion rates were occurring, as would be expected under aerated conditions.

To investigate the possibility of expansion under very low loads, a test stack of copper and cast-iron washers was set up under anoxic conditions with negligible applied load. The stack was placed in a nitrogen-purged glove box at room temperature and the load on the stack was reduced by minimising any frictional load between the central copper support rod, by reducing the diameter slightly, and supporting the load lever. The stack was mounted vertically and wetted by pumping test solution to the top of the stack and allowing it to drain down into a reservoir at the base. The duration of the wet and dry periods was altered during the course of the experiment to determine whether the length of the drying period had any effect on expansion rate. For comparison, a test was also carried out under low load in aerated conditions, using the same test stack directly exposed to the atmosphere, while applying wetting cycles of various durations.

For comparison with anoxic conditions, simple tests were also carried out under aerated conditions with a stack of 13 carbon steel and 13 copper washers that were mounted in air at room temperature and wetted with tap water using a timer-controlled pump system. The tap water was recirculated. The expansion was measured using a standard dial gauge placed at the top of the stack.

2.2 Analysis of corrosion products

Measurements were carried out to identify the composition of both the gaseous and solid products of the corrosion reactions proceeding in the stress cell, as follows.

2.2.1 Analysis of gaseous corrosion product

The gaseous products of the reactions were analysed by attaching an evacuated gas sample bomb to the outlet from Cell 3 (carbon steel, 10 MPa) during the first set of experiments and analysing its contents by mass spectroscopy.

2.2.2 X-ray photoelectron spectroscopy

The composition of the surface layer on selected carbon steel specimens was determined using X-ray photoelectron spectroscopy (XPS). In XPS the sample is irradiated with soft X-rays which causes core electrons to be ejected from the sample surface. A spectrum of the energies of these ejected electrons is produced. The electron energies of interest lie in the range 0–1500 eV. Because the escape depth of electrons at these energies is typically between 2 and 8 monolayers, XPS is surface specific. The binding energies (BE) of core electrons are dependent on the chemical state of the element and so it was possible to obtain elemental and chemical information using this technique. The analyser energy was selected to provide survey scans and detailed scans over the main peaks of interest. The area under the principal peak of each element in the spectrum, divided by an empirically derived sensitivity factor /16/, is proportional to the concentration of that element on the surface. The sensitivity of the technique is about 0.1 atomic percent, depending on the element.

The analysis was performed in a VG ESCALAB MkII, with a base pressure of 5×10^{-10} torr in the analysis chamber. The pressure during analysis was 1×10^{-8} torr. 200 Watt Al Kα radiation (1486.6 eV) was used to excite photoelectrons. Survey scans were performed with the analyser operating at a constant pass energy of 100 eV. Detailed scans were recorded with a pass energy of 20 eV. A 4 mm aperture was used as the entrance slit to the spectrometer enabling electrons to be collected from a 4 mm diameter area of the sample.

The samples were transported from the glovebox in an air-tight transport vessel and transferred in air quickly from the transport vessel to the fast entry port of the analysis instrument. It is probable that some aerobic oxidation occurred during the transfer procedure.

2.2.3 Scanning electron microscopy

The morphologies of the oxides on the corroded steel discs were examined using a Hitachi S-800 low voltage scanning electron microscope (LVSEM). This instrument has a high brightness field emission gun which gives imaging for accelerating voltages from 500 V to 25 kV. The low voltage capability of the instrument is useful in examining delicate materials because beam damage effects are minimised. A JEOL 840 scanning electron microscope was used to determine the elemental composition of the corrosion product using energy dispersive analysis (EDX).

2.2.4 Raman spectroscopy

The compositions of the corrosion products formed on carbon steel specimens were determined using Raman spectroscopy, an optical technique with which chemical and phase specific information can be obtained non-destructively and in situ, with a spatial resolution of 2–4 μm. A Renishaw Raman Microscope was used. Spectra were recorded in the back-scattered geometry. The exciting laser wavelength was 632.8 nm (from an air-cooled HeNe ion laser) and the power was approximately 20 mW. The intensity and position of the bands in a laser Raman spectrum depend both on the chemical composition and the crystal phase composition of the sample.

The test cells containing the specimens for Raman analysis were rapidly removed from the stress cell apparatus and transferred to a nitrogen-purged glove box, where the specimens were transferred to a gas tight glass cell containing an optical flat to permit access of laser light. This procedure ensured that oxidation of the corrosion product was minimised.

2.2.5 XRD

X-ray diffraction (XRD) analysis was carried out using a fully automated Siemens D500 powder diffractometer employing copper Kα radiation (λ=0.15406 nm) and a secondary monochromator. XRD identifies the crystalline components present in a sample by comparing the diffractogram peak positions against a database of XRD patterns from known materials.

2.3 Measurement of oxide mechanical properties

2.3.1 Preparation of corroded specimens

Polished, flat 7 mm square coupons of carbon steel (BS4360 grade 43A) and cast iron (wt% C 3.7; Si 2.77; Mn 0.07) were prepared. They were pickled to remove air formed oxides using the same method as used for the stress cell specimens. The samples were then corroded in two artificial anoxic groundwaters at 50°C and 85°C. One groundwater had the same composition as that used for the stress cell experiment, and the other, referred to as the 'low pH' groundwater had the following composition (mM): Na^+ 131.3; K^+ 0.19; Ca^{2+} 109.5; Mg^{2+} 2.06; Cl^- 339.6; SO_4^{2-} 7.40; pH 7–8.

The specimens were placed in alumina crucibles (for neutral pH groundwater) or zirconia crucibles (for alkaline groundwater) containing the appropriate test solution, to avoid silicate contamination from glass. The samples were then sealed inside glass vessels that were immersed in oil baths at the appropriate temperatures. The samples were removed after ~8500 hours, inside a nitrogen-purged glovebox, and transferred in gas-tight vessels to the atomic force microscope (AFM) for examination. The samples were examined under the test groundwater in a nitrogen-flushed environment.

2.3.2 Atomic Force Microscopy

The Atomic Force Microscope (AFM) technique involves scanning a tiny, micro-machined probe across the surface. The instrument detects forces developed at an atomic scale between the tip of the probe and the sample surface, so that topographic images can be obtained with a height resolution of less than 1 Å /7/. The AFM was used to obtain a qualitative assessment of the hardness of the very thin corrosion product films. An East Coast Scientific (ECS) AFM equipped with a 16 μm tube scanner was employed using a Si_3N_4 microlever with a nominal spring constant, k, of 0.01 N/m. The AFM was operated in the force versus distance mode (F-d) whereby the approaching/retracting tip senses interactions at the interface with the surface. Tip displacement was measured using a laser and a position sensitive photo-diode detector. The samples were examined under liquid in a nitrogen-flushed environment. No images were taken. Material properties can be extrapolated from the F-d curves.

The general features of the approach and retract F-d curves in AM analysis are shown in Figure 2-6. The horizontal sections represent the undeflected state of the lever when the tip is far away from the surface. The approach curve generally exhibits a small excursion into the net attractive force regime where the strong short-range surface adhesive interactions are felt by the tip. When the effective force constant of the interaction is greater than that of the lever, the tip 'snaps' into contact. Further travel by the specimen stage in the z-direction brings the tip-surface interaction back into the net repulsive force regime; the distance travelled by the stage to obtain zero deflection represents the size of the adhesive interaction. The steep rise in the approach curve then reflects the increasingly large relative deflection of the lever as the incremental relaxation of the surface per unit additional applied force decreases due to the spreading of

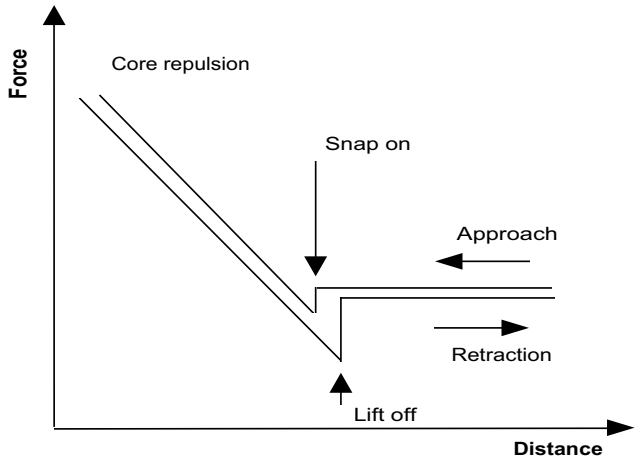

Figure 2-6. *Typical F-d curve from a classical hard surface.*

the load over a successively greater tip-to-surface contact area. The slope of this curve is a measure of the rigidity or stiffness of the system. Curvature at the point of contact is indicative of deformation of the surface by the tip, thus the contact area of the tip on the surface changes as a function of applied force as shown in Figure 2-7.

The retract curve substantially retraces the approach curve, but the adhesive interaction is now larger due to the much larger contact area arising from the maximum loading of the tip. The asymmetry in the snap-on and lift-off forces, and the extent to which deformations do not recover elastically, are the major causes of hysteresis in the approach-retract cycle.

Trial measurements were carried out using the AFM to look at the following materials: a well characterised hard surface (gold film on silicon), a glass slide which was exposed to 0.1 M NaOH solution for ~1 week, a cast iron coupon corroded anaerobically in artificial ground water (this sample was immersed in deaerated groundwater when measured) and a piece of mild steel which had been exposed to aerated 0.1 M NaOH for approximately 3 years. Force-distance measurements were made and it was found that the oxide layer on the steel was considerably less hard than the layer on glass. These tests demonstrated that hardness measurements could be successfully made using the AFM.

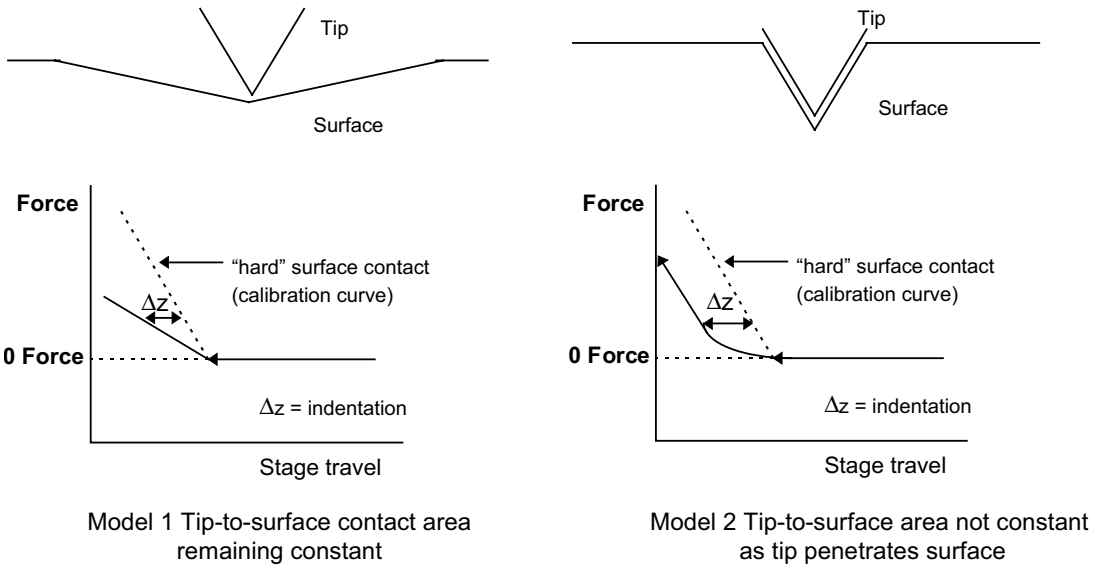

Figure 2-7. *Two models for the indentation of a surface with an AFM tip.*

2.4 Nano-indentation

A Fischer Ultra Low Load hardness instrument was used to perform indentation measurements. This measures the movement of a diamond stylus in contact with a surface. For indentation measurements the stylus is impressed into the surface under the influence of an increasing load. After reaching a predetermined maximum value the load is reduced and the penetration depth decreases due to elastic recovery of the deformed material. The depth and load are monitored continuously which allows both Hardness and Young's Modulus data to be derived. This is depicted graphically in Figure 2-8. The depth versus load raw data can be fitted to a power law expression to obtain hardness as a function of depth and load, as well as Young's Modulus and hardness at zero load extrapolated from the first 20% of the unloading data curve. The technique was tested using a sample of carbon steel corroded aerobically in 0.1 M NaOH and a single crystal of magnetite (Fe_3O_4) as a reference surface.

Results

2.5 Stress cell experiments

During the experiment the following parameters were monitored for each test cell:

- load on stack of specimens,
- position of transducer on lever arms,
- gas pressure in test cells,
- temperature of test solutions.

These parameters were recorded automatically using a PC-based datalogging system and by taking manual readings from the panel meters in the control panel. Two transducers were used on Cell 3 to ensure that the experiments would produce results even if one transducer failed, as this was regarded as the most important cell.

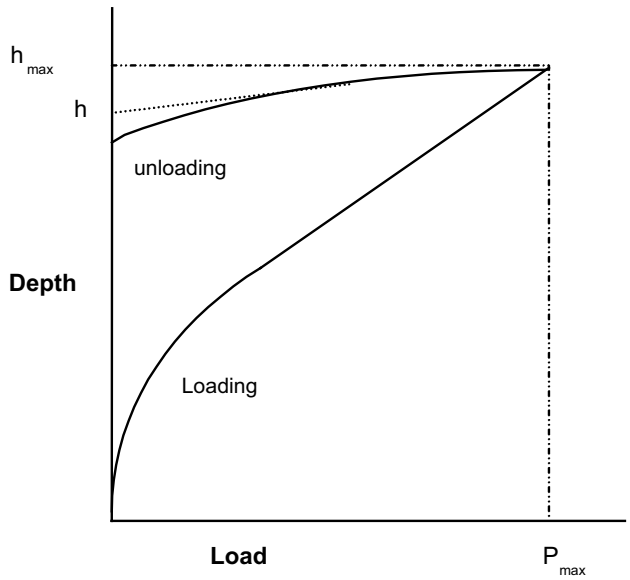

Figure 2-8. *Schematic nano-indentation depth-load curve.*

2.5.1 First series of stress cell experiments

Initially three cells were set up; two contained alternate mild steel and copper discs, at compressive loads of 1 MPa and 10 MPa. The third, control cell, contained interleaved stainless steel and copper discs (i.e. Cell 1 – stainless steel/copper, 10 MPa; Cell 2 – carbon steel/copper, 1 MPa; Cell 3 – carbon steel/copper, 10 MPa). The change in the actual load on the specimen stacks and the change in the displacement of the transducers at the end of the lever arms of the three test cells are shown in Figure 2-9 and Figure 2-10. There was a relaxation in the load of all three cells; the reason for this is not clear. There was a contraction on the displacement transducer on the stainless steel stack of 1.38 mm, corresponding to a change in a single specimen surface of 0.43 µm but the height of the stacks containing the mild steel remained virtually constant.

The initial corrosion potentials of the carbon steel wires in the test cells were –600 to –630 mV vs AgCl, but they fell within a day to –800 mV to –850 mV, and then again to –880 mV within a week. These potentials indicate that anaerobic corrosion was occurring. The edges of the carbon steel specimens were seen to go black during the experiments, which is also consistent with anaerobic corrosion occurring. It is probable that any residual oxygen in the cell when it was sealed would have been consumed by corrosion of the metals in the test cell and pipework. In the long-term failure of the reference electrodes occurred and no further potential measurements could be made. It is probable that this was due to dissolution of the silver chloride on the surface of the reference electrode.

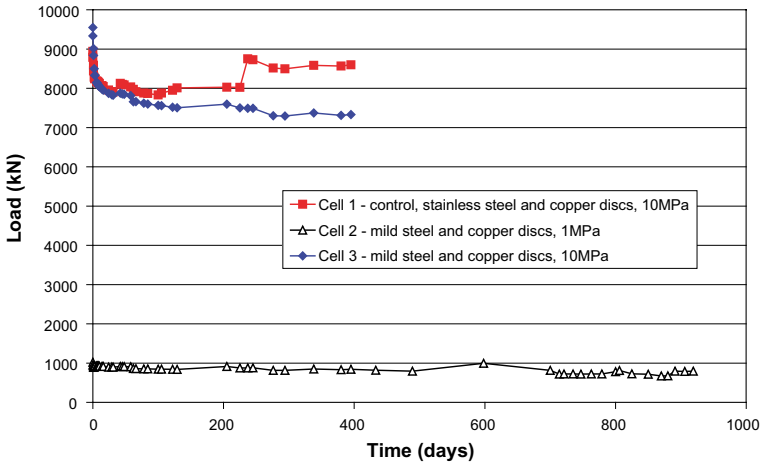

Figure 2-9. *Change in load on stress cells, first series, high pH artificial groundwater, 69°C.*

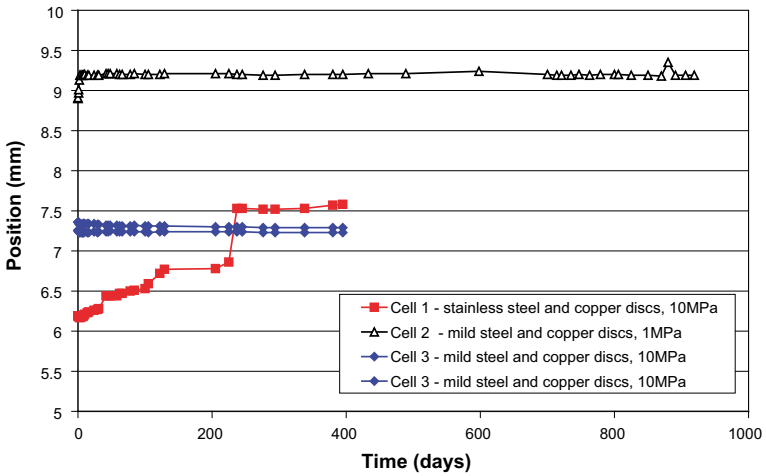

Figure 2-10. *Change in displacement on stress cells, first series, high pH artificial groundwater, 69°C.*

2.5.2 Second series of stress cell experiments

After 380 days' operation, test cells 1 and 3 (cell 1: stainless steel/copper, 10 MPa and cell 3: carbon steel/copper, 10 MPa) were dismantled and the specimens examined. The remaining cell (cell 2: carbon steel/copper, 1 MPa) was left running for a total of 870 days.

Cell 3 was set up again using carbon steel and copper discs at ~1 MPa load using demineralised water as the test solution, open to the atmosphere (i.e. the test solution was aerated), with the aim of demonstrating that rapid corrosion would lead to expansion in the test rig. The carbon steel disks were freshly prepared and the copper disks were recovered from the previous experiments and cleaned in acid before use. The results of these experiments are shown in Figure 2-11. The potential of the steel electrode with respect to the silver chloride reference electrode was consistent with the solution being oxygenated (ca –30 mV vs Ag|AgCl). Although the test specimens in the naturally aerated demineralised water were clearly corroding, no expansion was observed after 49 days. This may be because at the load that was being applied, any corrosion product that formed was lost through the channels of the copper discs. The level of water in the test cell was reduced so that the specimens were partly exposed to a humid atmospheric phase, rather than an aqueous one, with the aim of reducing the possibility of removing corrosion product in the aqueous phase. No expansion was observed under these conditions either. The load was reduced further by removing the second lever arm, to give a load of 450 kPa, but still no expansion occurred.

Cell 1 was set up again using cast iron specimens in deoxygenated conditions. The test conditions were as before (i.e. 69°C, bentonite-equilibrated groundwater) but no expansion was observed (Figure 2-11).

2.5.3 Low load expansion experiments

In parallel with the experiments with the stress cell a simple experiment using an unloaded stack of 13 copper discs and 13 steel discs specimens exposed to tap water was set up to see whether any expansion could be measured in an unloaded system with a high corrosion rate. In the first test the stack was wetted for 12 hours during each 24 hour period and no load was applied. The total expansion for a single iron surface and the cumulative expansion rate for a single iron surface (based on the total expansion divided by the total elapsed time), are shown in Figure 2-12. In a subsequent test, small loads were applied (~0.9 kg, followed by ~1.5 kg) and the test stack was wetted for 0.5 hours in every 24 hour period. The results from this test are shown in Figure 2-13.

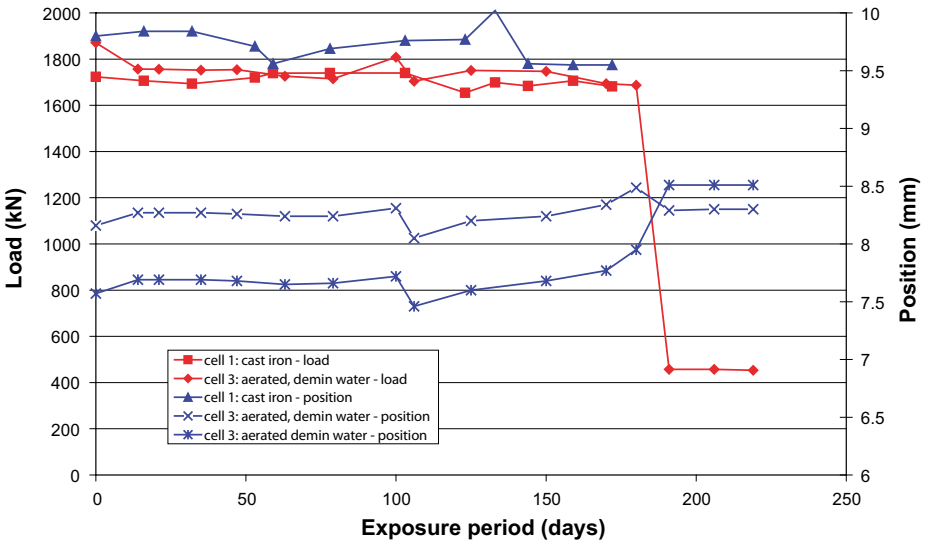

Figure 2-11. *Results of second series of stress cell experiments at 1 MPa load (note: cell 3 had two position transducers).*

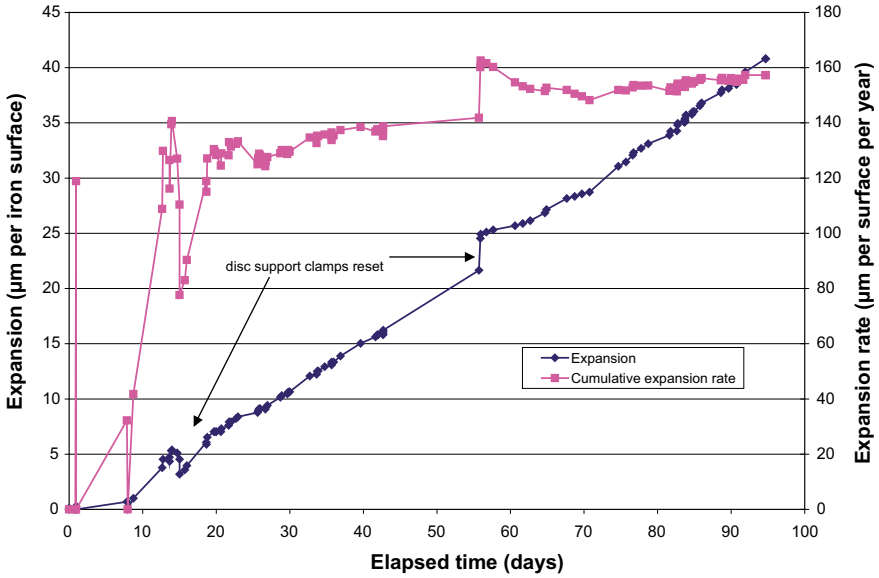

Figure 2-12. *Results from first test on stack of copper and steel discs (13 of each) in aerated demineralised water, wetted for 12 hours every 24 hour period, no applied load.*

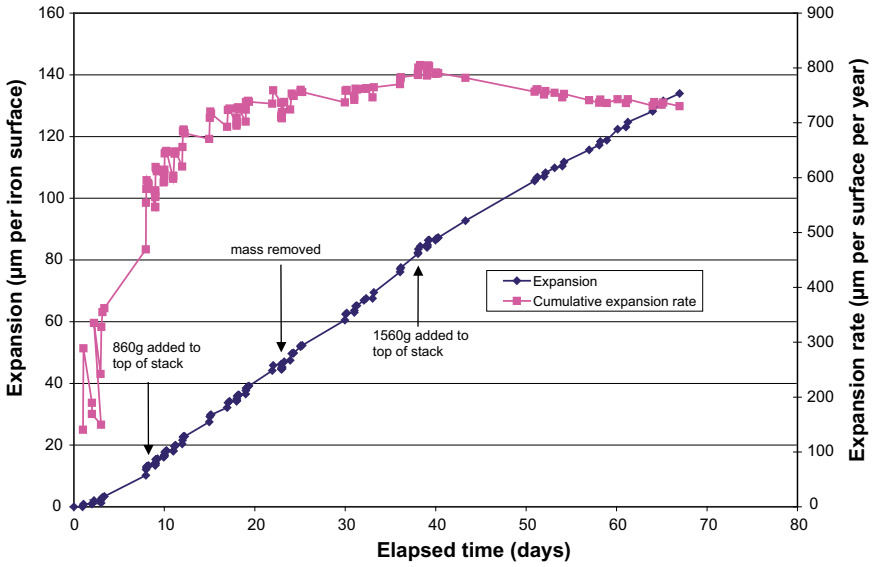

Figure 2-13. *Results from second test on stack of copper and steel discs (13 of each) in aerated demineralised water, wetted for 0.5 hours every 24 hour period, with applied loads as shown.*

The experiment using a low applied load on the stress cell stack inside an anoxic glovebox with intermittent wetting did not produce any expansion (Figure 2-14). The wetting regime was changed during the course of the experiment from 12 hours on and 12 hours off to full immersion but no expansion was observed under any wetting conditions.

The stack was then removed and placed in aerated solution under low load conditions and the wet-dry cycling was repeated. No expansion was observed (Figure 2-15 and Figure 2-16) until the load on the stack was minimised, by removing all frictional restrictions in the form of the O-ring sealed plug in the end of the environmental chamber and the central copper supporting rod, when an expansion of 0.2 mm was measured over a period of ~80 days (Figure 2-17).

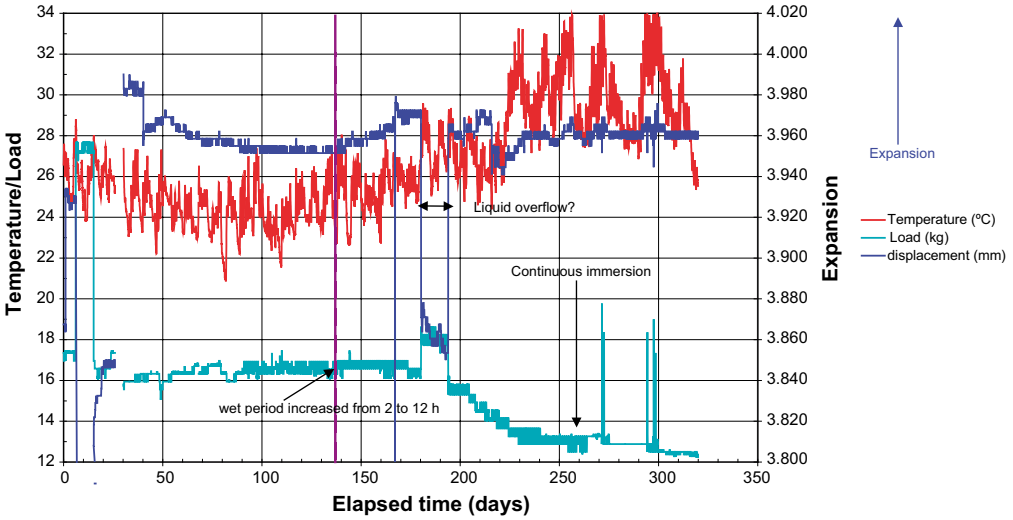

Figure 2-14. *Results from expansion experiment using stress cell in nitrogen-purged glove box, with intermittent wetting of test stack by high pH groundwater.*

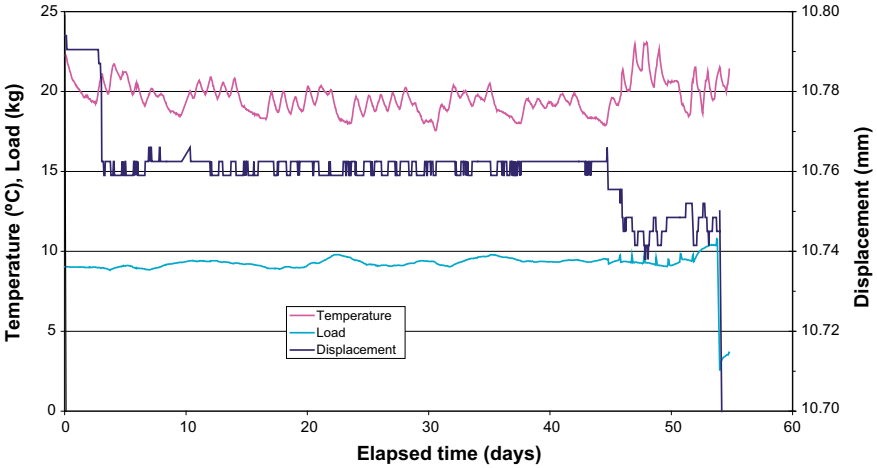

Figure 2-15. *Results from expansion experiment using stress cell fully exposed to atmosphere with low load – total immersion in high pH groundwater.*

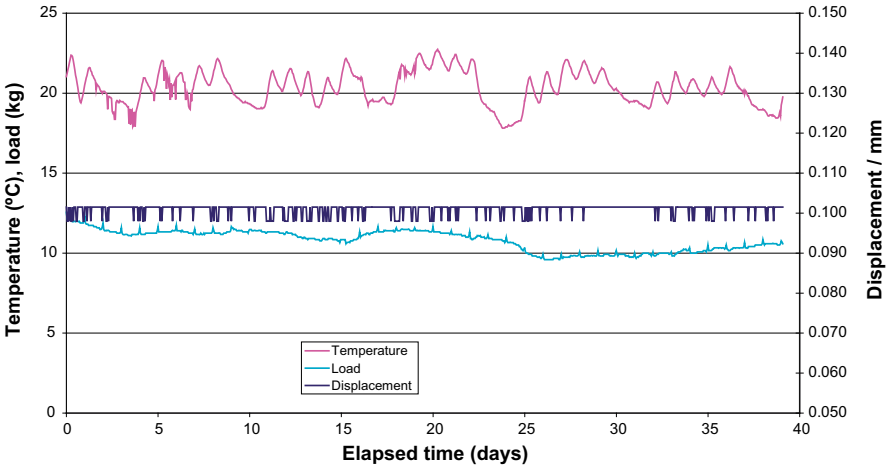

Figure 2-16. *Results from expansion experiment using stress cell fully exposed to atmosphere with low load – intermittent wetting of test stack wetting of test stack by high pH groundwater (2 hours wet, 22 hours dry), top plug removed.*

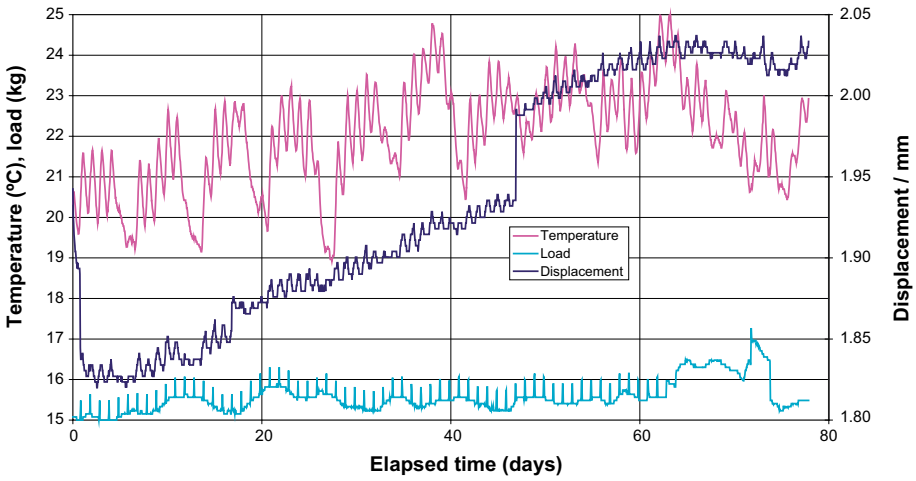

Figure 2-17. *Results from expansion experiment using stress cell fully exposed to atmosphere with low load – intermittent wetting of test stack wetting of test stack by high pH groundwater (2 hours wet, 22 hours dry), top plug removed, fill tube repositioned and central bar removed.*

2.6 Analysis of corrosion products from stress cell experiments

2.6.1 Visual inspection

Two of the cells from the first set of stress cell experiments, namely the cell containing the stainless steel control stack (Cell 1) and the cell containing carbon steel (Cell 2) at 10 MPa, were dismantled after they had been operating for 380 days and the samples were removed and inspected visually. A black corrosion product was visible on the surfaces of the carbon steel discs, both around the edge of the specimens and on the surfaces in contact with the copper. The stainless steel specimens in Cell 1 remained shiny although some black corrosion product had formed on the carbon steel end plugs and this had spread to the outer edges of the disks. The appearance of the specimens is shown in Figure 2-18.

Figure 2-18. *Appearance of specimens from Cells 1 (stainless steel control) and 3 (carbon steel) after exposure to artificial groundwater for 380 days at 69°C (first series). The stack of specimens can be seen at the top and the cell end plugs at the bottom.*

Photographs of the specimens at the end of the second series of experiments are shown in Figure 2-19 (deaerated, cast iron) and Figure 2-20 (aerated, carbon steel). The deaerated cast iron specimens were uniformly black across the mating surfaces and along the outside edges. The aerated specimens had orange-brown corrosion product on the edges, but were black on the mating surfaces, suggesting that oxygen access was restricted in the crevices. Tests in fully aerated conditions under low load became bright orange (Figure 2-21).

Surface profilometry measurements on the surface of one of the copper specimens showed no flattening of asperities.

Figure 2-19. *Appearance of test stack at end of experiment with cast iron (Cell 1, second series of tests).*

Figure 2-20. *Aerated stress cell test with demineralised water, 69°C, second series of experiments, Cell 1.*

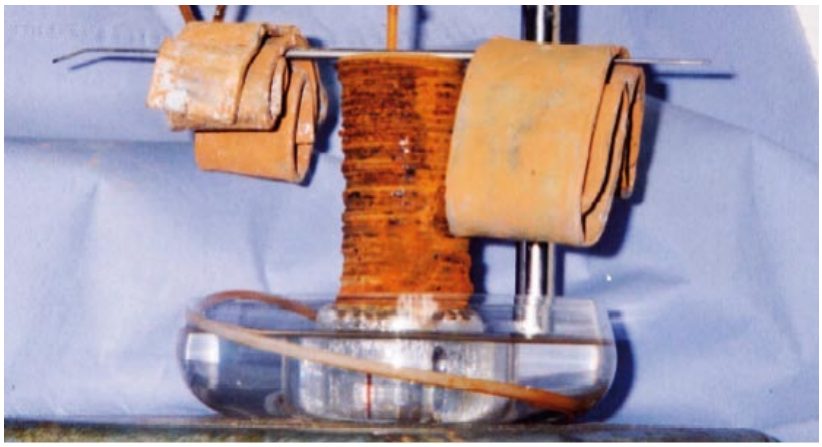

Figure 2-21. *Appearance of specimens at the end of the fully aerated expansion tests.*

2.6.2 Analysis of gaseous corrosion product

Mass spectral analysis of the gas sample taken from cell 3 from the first sequence of tests showed that the gas contained approximately 3% hydrogen in nitrogen. The presence of hydrogen confirms that the carbon steel was corroding anaerobically.

2.6.3 Scanning electron microscopy and EDX analysis

Scanning electron micrographs were obtained for the deposit on an anaerobically corroded carbon steel disc from Cell 3 (first series), as shown in Figure 2-22 and Figure 2-23. The low magnification image (Figure 2-22) shows an extensive deposit, although it was not a contiguous film. Higher magnification imaging (Figure 2-23) of the deposit shows that the deposit was composed of smooth 'particles' ca 5 to 10 microns in size on a background of very small particles (<< ca 1 micron). The EDX spectrum obtained from the deposit showed that silicon, sulphur and chlorine were present, in addition to iron.

Scanning electron micrographs were also obtained for the surface of anaerobically corroded cast iron (Cell 1, second series) and aerobically corroded carbon steel samples (Cell 3, second series). The images are shown in Figure 2-24 and 2-25. The EDX spectrum from the cast iron sample showed sodium, chlorine and silicon to be present in addition to the predominant peaks of iron and oxygen. This sample had a higher level of carbon than the mild steel sample, which contained peaks for iron, oxygen, copper and chromium, but not sodium or chlorine.

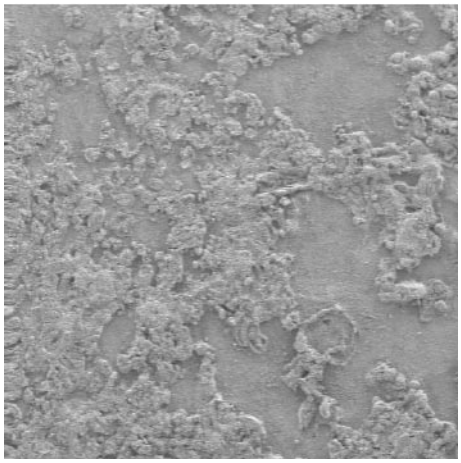

Figure 2-22. *LVSEM image of carbon steel sample from cell 3 (×200).*

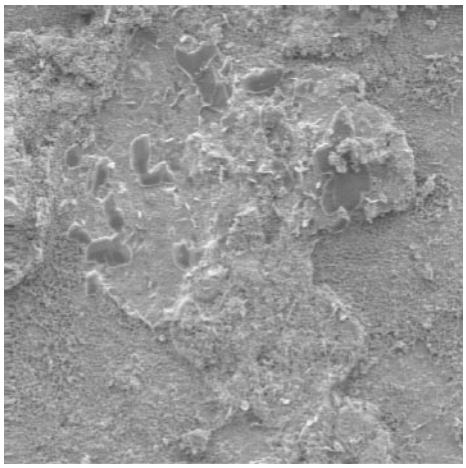

Figure 2-23. *LVSEM image of carbon steel sample from cell 3 deposit showing smooth regions on a background of very small particles (×1700).*

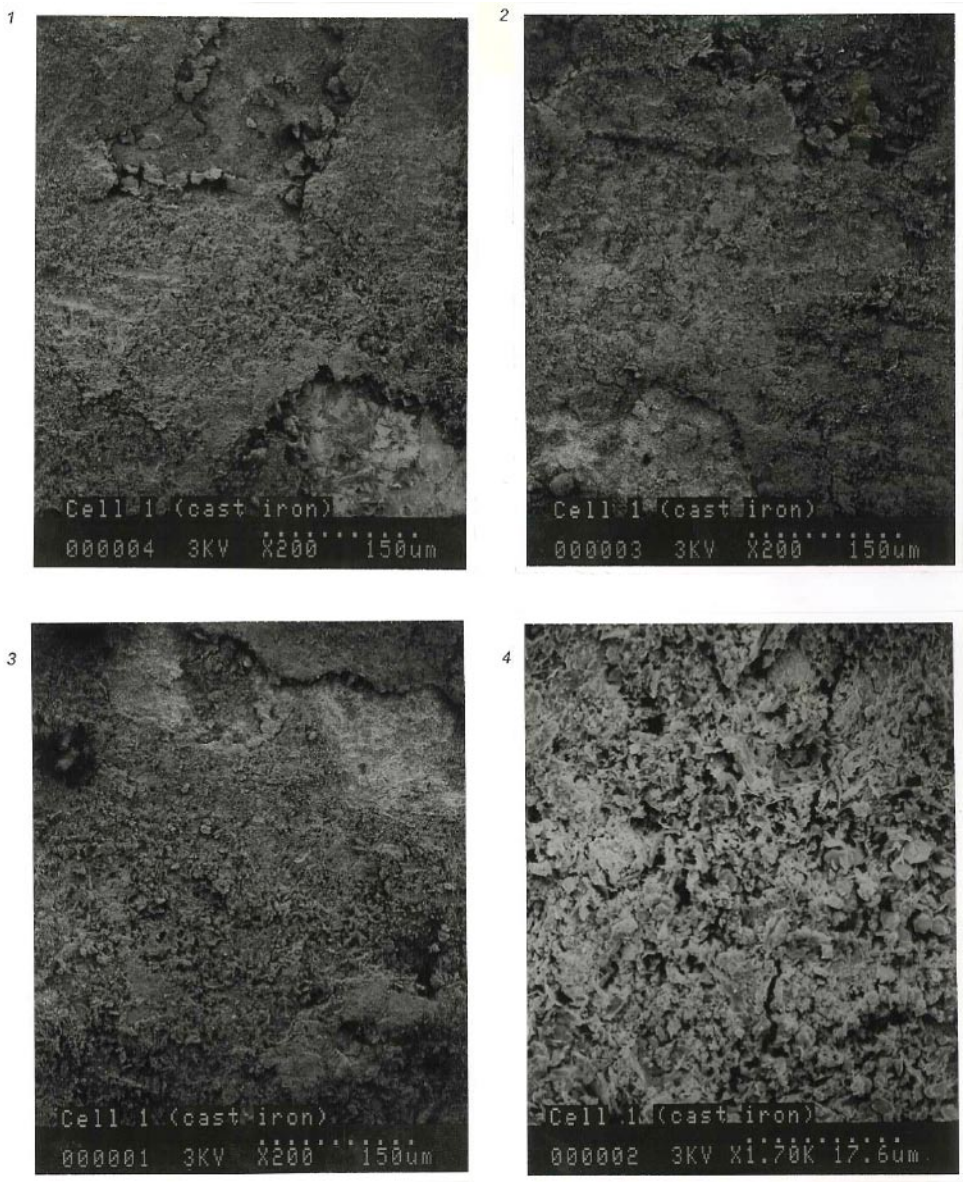

Figure 2-24. *LVSEM images of anaerobically corroded cast iron (Cell 1, second series) specimens.*

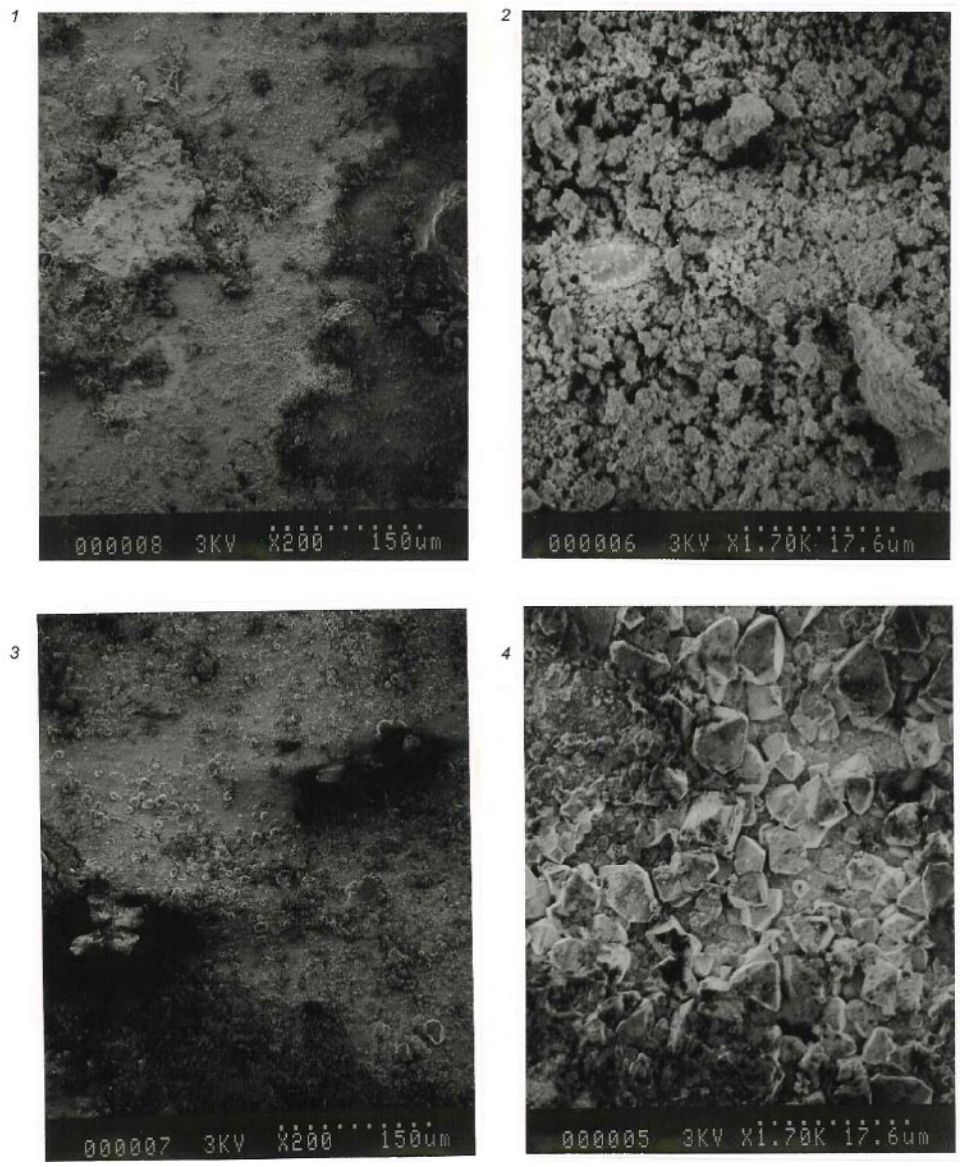

Figure 2-25. *LVSEM images of aerobically corroded carbon steel samples (Cell 3, second series).*

2.6.4 Raman spectroscopy

The Raman spectrum obtained from the black areas of an anaerobically corroded carbon steel sample (Cell 3, first series) was characteristic of magnetite Fe_3O_4 (Figure 2-26). Raman analysis also detected magnetite on an anaerobically corroded cast iron specimen (Cell 1, second series). The predominant phase detected on the aerobically corroded carbon steel sample (Cell 3, second series) was Fe_2O_3, although Fe_3O_4 (magnetite) was also present.

2.6.5 X-ray diffraction

XRD analysis of an anaerobically corroded cast iron specimen (Cell 1, second series) and an aerobically corroded carbon steel specimen (Cell 3, second series) detected magnetite on both samples. A hydrated iron carbonate was also present on the cast iron sample.

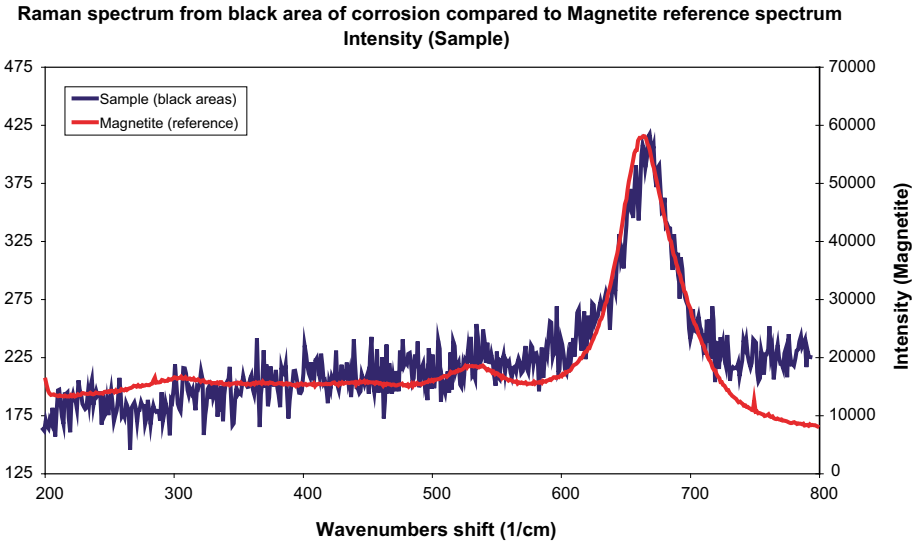

Figure 2-26. *Raman spectrum for carbon steel disc from anaerobic corrosion expansion experiment in Cell 3 (first series, 69°C, high pH groundwater).*

2.6.6 X-ray Photoelectron Spectroscopy

The XPS analysis of an anaerobically corroded carbon steel sample (Cell 3, first series) detected oxygen, carbon, iron, chlorine, silicon and sodium. This analysis reflects the presence of an oxide film whose surface is contaminated with solutes from the test solution. From the detailed scans the predominant species detected were FeOOH and Fe_2O_3 (goethite and haematite). This result indicates that some oxidation of the corrosion product surface had occurred during transfer of the specimen to the spectrometer. The presence of silicon is believed to be due to residual glass beads from peening the surface of the copper discs.

2.7 Oxide mechanical properties

Eight samples were corroded in four cells under various conditions as detailed in Table 2-3. The samples were transported for analysis under dry nitrogen. All the samples were supplied "wet", except for two early samples, which were supplied pre-dried for an early trial run. Two of the four test cells containing carbon steel and cast iron test coupons in low pH water and bentonite-equilibrated groundwater were broken open in an anoxic glove box (two cells at 50°C, two cells at 80°C), after ~11 months spent corroding. Some loose corrosion product was suspended in the test solution. On removal of the corrosion coupons from the test environments the cast iron samples were found to have thick fluffy black deposits in some areas, whereas the carbon steel had a much thinner oxide, with some shiny metal visible beneath a thin black coating. The appearance of the specimens is summarised in Table 2-4.

XPS analyses were carried out on samples prepared for mechanical property measurements. A summary of the results from the XPS analysis is given in Table 2-5. Detailed examination of the Fe 2p region (see Figure 2-27) allowed the oxidation state of the predominant Fe ionic species to be determined. The presence of a distinct shake up satellite peak /16/ in the Fe 2p region is indicative of Fe(II). The Fe peaks were clearer on the carbon steel samples than on the cast iron samples, which is consistent with a low density layer on the cast iron samples. By examination of the O 1s region it is possible to differentiate between oxide and, for example, water. Despite the high vacuum of the XPS instrument, water was still detectable in most cases. This would tend to suggest that XPS analysis did not degrade the samples.

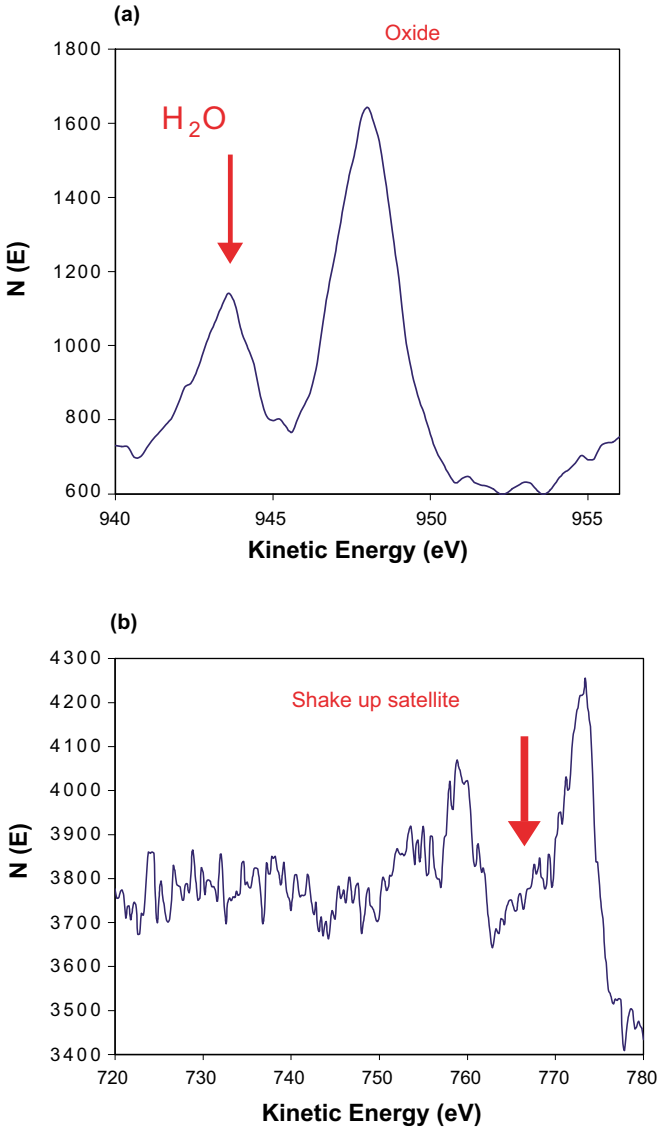

Figure 2-27. *Detailed XPS spectra obtained from (a) carbon steel and (b) cast iron corroded at a temperature 80°C in high pH, Bentonite equilibrated ground water.*

Table 2-3. Details of samples prepared for AFM measurements.

Sample	Temperature (°C)	Groundwater	Material	How analysed
1	80	high pH	carbon steel	Wet
2	80	high pH	cast iron	Wet
3	50	high pH	carbon steel	Wet
4	50	high pH	cast iron	Wet
5	80	low pH	carbon steel	Wet
6	80	low pH	cast iron	Wet
7	50	low pH	carbon steel	Dry
8	50	low pH	cast iron	Dry

Table 2-4. Appearance of corroded specimens used for characterisation of oxide mechanical properties.

Material	Low pH, 50°C	Low pH, 80°C	High pH, 50°C	High pH, 80°C
Cast iron	Orange-brown corrosion product*	Black coating, black particulate in solution	black	black
Carbon steel	Orange-brown*	Black coating, black particulate in solution	black deposit, but some areas still shiny	Black deposit, but some areas still shiny

*Specimens used to check analytical procedure, probably had air in cell.

Table 2-5. Summary of XPS analyses of samples corroded in artificial groundwaters.

Temp (°C)	Groundwater	Material	Fe (II)	Water
80	high pH	carbon steel	yes	yes
80	high pH	cast iron	more prominent shake up satellite	yes
50	high pH	carbon steel	yes but different background	no
50	high pH	cast iron	s/n too poor	no
80	low pH	carbon steel	yes	no
80	low pH	cast iron	yes	yes

Typical examples of the F-d curves obtained from samples immersed in the test groundwaters are shown in Figure 2-28 and Figure 2-29 and the shape of the F-d curves points to the second model in Figure 2-7 being applicable, which is that the tip penetrates a compliant layer and as a result the tip-to-surface area is not constant. Typical F-d curves from the dry samples are shown in Figure 2-28. The F-d curves obtained from the wet samples (i.e. samples 1 to 6) are similar in form. Typical examples are shown in Figure 2-29. From the F-d curves it is possible to determine an indentation distance versus load plot (Figure 2-30 shows a typical example corresponding to the F-d data in Figure 2-29). It is therefore possible to determine the Young's modulus of the layer being probed and estimate its thickness. These data, for the "wet" samples, are summarised in Table 2-6.

Table 2-6. Properties of oxide layers calculated from AFM F-d curves.

Temp (°C)	Groundwater	Material	Thickness	Young's Modulus
80	high pH	carbon steel	ca 20–60 nm	ca 1–2 × 106 Pa
80	high pH	cast iron	>5 µm	ca 4 × 104 Pa
50	high pH	carbon steel	few 10s nm	–
50	high pH	cast iron	>1 µm	ca 5 × 105 Pa
80	low pH	carbon steel	ca 20–30 nm	–
80	low pH	cast iron	ca 100–300 nm	ca 5 × 105 Pa

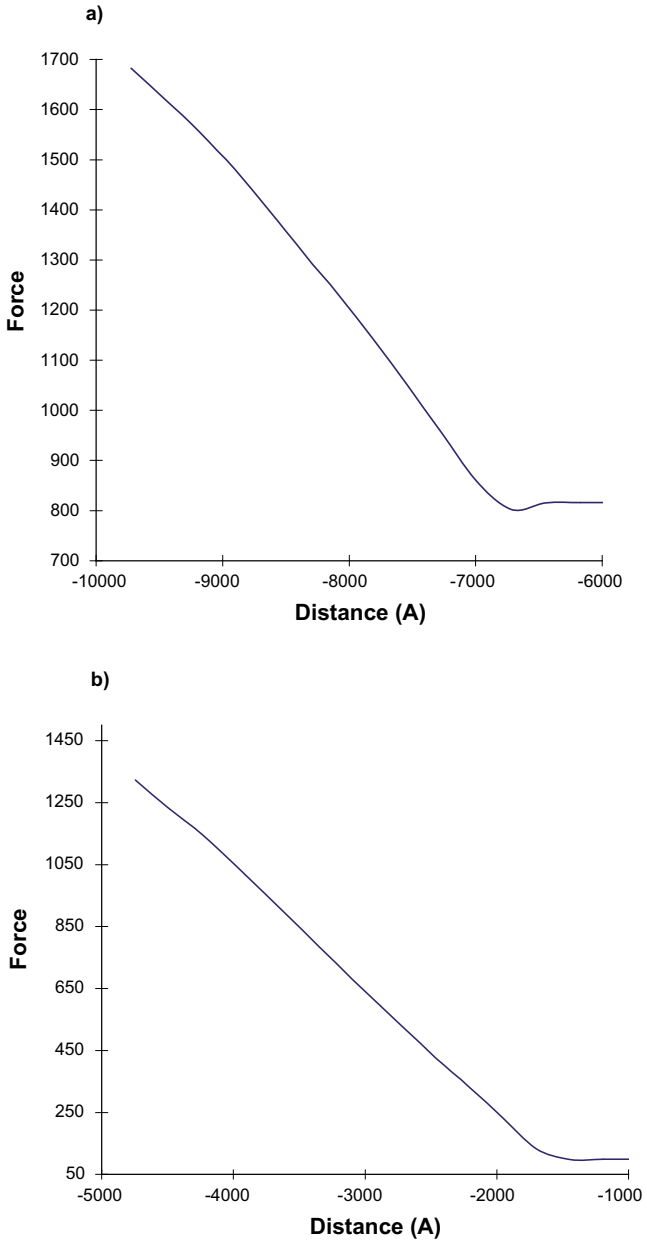

Figure 2-28. *Typical AFM F-d curves obtained from the dry samples (numbers 7 and 8): (a) carbon steel and (b) cast iron, corroded at 50°C in low pH, ground water.*

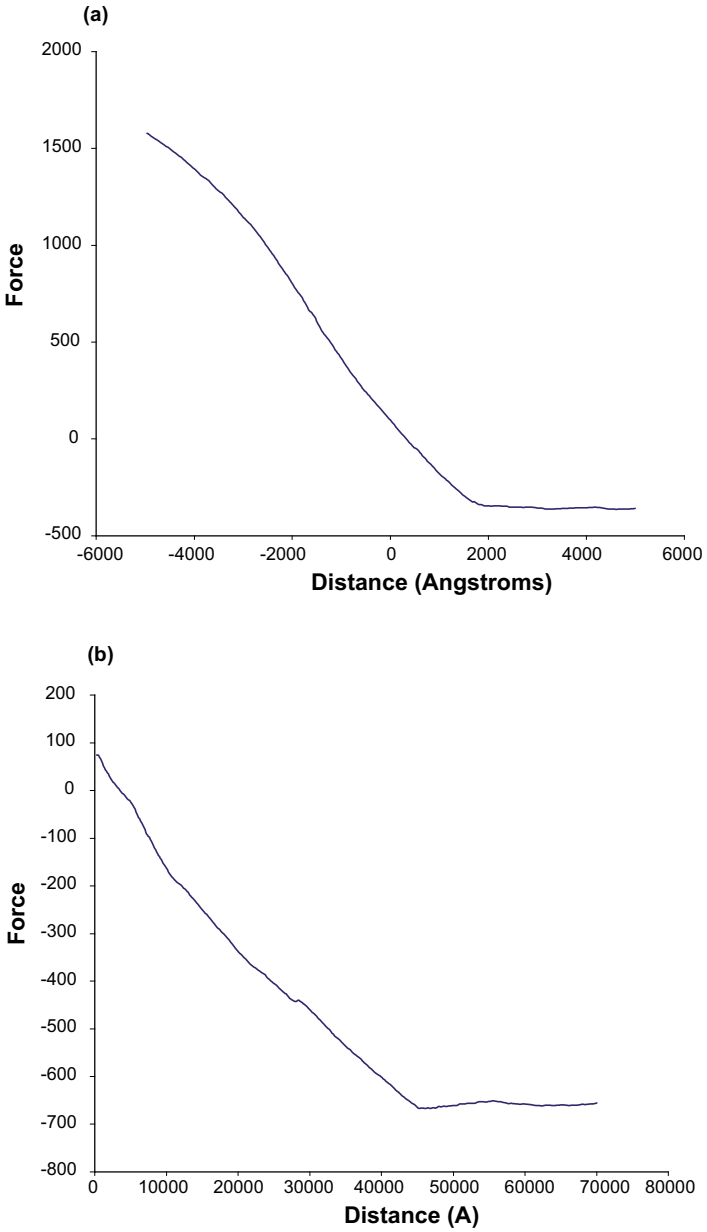

Figure 2-29. *Typical AFM F-d curves obtained from samples 1 and 2: (a) carbon steel and (b) cast iron corroded at a temperature 80°C in high pH, bentonite equilibrated ground water.*

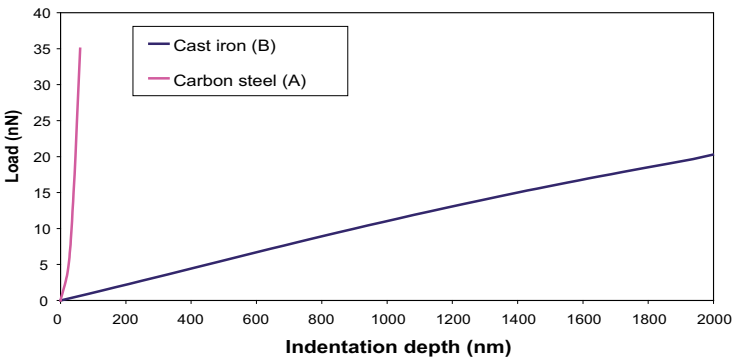

Figure 2-30. *Typical plot of load vs indentation depth calculated from the measured AFM F-d curves for samples of cast iron and carbon steel corroded at 80°C in high pH, bentonite equilibrated ground water. The F-d curves from the same samples can be seen in Figure 30.*

2.8 Nano-indentation

Table 2-7 lists the measured values for hardness and Young's modulus and compares these to literature values for cast iron and the minerals magnetite (Fe_3O_4) and hematite (Fe_2O_3). It is clear from the high load indentation of the aerobically corroded sample that there are three layers being sampled as the probe travels over three microns into the sample surface. An idealised picture of the layers is presented in Figure 2-31. Each region is characterised as (1) a soft thin layer, (2) a hard 'coating', and (3) substrate. The response of the Fe_3O_4 single crystal approached a hardness value of 5000 N mm^{-2} at 100 N load which is consistent with published data and with the value obtained for the hardness of layer 2 in Figure 2-31.

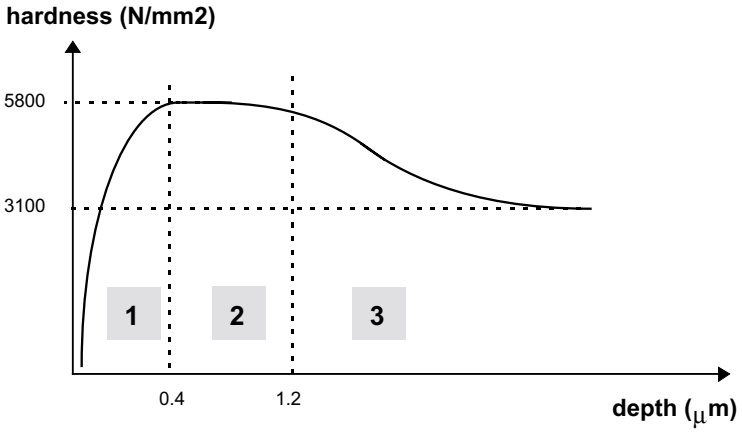

Figure 2-31. *Idealised plot of indentation measurement on aerobically corroded cast iron surface.*

Table 2-7. Data from nano-indentation measurements on various oxides under oxic conditions.

Sample	Hardness, H (MPa)[a)]	Young's Modulus, E (GPa)
Corroded carbon steel (100 g)	4,100	180 [a)]
Corroded carbon steel (10 g)	8,124	187 [a)]
Fe_3O_4 single crystal (10 g)	7,361	166 [a)]
Cast iron [b)]	1,500–2,600	100–176
Magnetite (Fe_3O_4) [c)]	5,000–7,200	
Hematite (Fe_2O_3) [c)]	4,300–5,600	

[a)] as measured

[b)] C.J. Smithells, Metals Reference Book, Butterworths

[c)] Handbook of Chemistry and Physics, The Chemical Rubber Company

3 Discussion

3.1 Corrosion-induced expansion

The aim of the stress cell experiments was to measure the amount of expansion caused by corrosion of iron or carbon steel in contact with copper surfaces, under a range of applied loads. The fact that expansion was measured when a stack of washers was fully exposed to fully oxygenated conditions with low applied loads demonstrate that the experimental approach used in the stress cell experiment is capable of detecting corrosion-induced expansion with a high sensitivity (e.g. Figure 2-17), as has been demonstrated by other workers /11–13/.

However, in the stress cell experiments with carbon steel and cast iron under deoxygenated conditions, in artificial groundwater and under loads representative of the repository situation, no expansion occurred, even though corrosion product analysis identified the presence of both hydrogen and black magnetite and the electrochemical potential of carbon steel reached highly negative values, confirming that anaerobic corrosion was taking place. When the loads were reduced to values well below those expected in the repository situation, no expansion was observed. No expansion was observed with cast iron specimens, where a thicker more voluminous oxide than on carbon steel was formed. It was also found that no expansion occurred when a loaded stress cell stack was exposed to aerated conditions, where much more rapid corrosion (ca 100 μm/yr cf 1 μm/yr) would have occurred. This may have been due to the restricted access of oxygen to the surfaces, as a result of the confined geometry in the crevice between the washers, leading to the formation of an oxide similar to that formed in deaerated solution.

The reason for the lack of any detectable expansion in the stress cell experiments is probably because the corrosion product was easily compressed or extruded from the copper-steel interface and it was not capable of withstanding the applied loads. Scanning electron microscopy showed that the anaerobic corrosion product was finely divided and it had deformed to fit into the available spaces between the discs in the stack of specimens, rather than forcing them apart. It is probable that the surface roughness and the grooves in the copper discs were filled with corrosion product from the anaerobic corrosion of the steel. This situation is in contrast to that experienced in concrete or in heat exchangers where jacking effects can cause severe mechanical disruption of the surrounding structures.

One possible reason for the low mechanical strength of the corrosion product formed at low temperature under anaerobic conditions is the higher proportion of water, in contrast to the situation in concrete where the supply of water is limited and high expansive stresses are formed, or to the oxide films formed at high temperature which have a much higher hardness /17/ and a lower water content. The XPS analysis (Table 2-5) demonstrated that water was present in the oxide films formed under aqueous immersion in deaerated artificial groundwater.

The lack of any accelerated corrosion at the junction between the copper and ferrous material indicates a lack of any galvanic effects and this is consistent with the results of recent electrochemical investigations of galvanic corrosion /18,19/, which showed that in the absence of oxygen there is negligible risk of galvanic corrosion at copper-cast iron couples in artificial groundwater.

In the stainless steel-copper control cell some contraction of the stack took place. The contraction may have been due to creep of the copper at asperity tips on the roughened copper surface, although microscopic examination of a copper specimen removed from the test did not reveal any significant flattening.

3.2 Oxide mechanical properties

Analysis of the corroded coupons (Table 2-6) showed that anaerobic corrosion of cast iron produced a thick (>5 μm) compressible, friable layer, but a thinner (<100 nm), less compressible layer on carbon steel. Previous work /6/ has shown that the corrosion product film on carbon steel in synthetic groundwater has a two-layer structure, with an adherent, compact film adjacent to the metal surface and a more friable, loosely adherent upper layer. In previous measurements /5/ it was found that cast iron produced hydrogen at a slightly lower rate than carbon steel and it is therefore unexpected to find more corrosion product on cast iron specimens. This may because the materials used previously for the gas generation rate measurements were not polished and it is possible that surface preparation had an influence on the thickness of the oxide film produced on the surface of the ferrous material.

The AFM measurements provided values of Young's modulus, E, for the predominantly magnetite films formed by anaerobic corrosion on cast iron or carbon steel; the compressibility is the inverse of the Young's modulus. This information could be used in any future finite element analyses to determine the force exerted by the iron oxide as it grows, assuming that the composition and structure of the film formed over a period of a few months in the laboratory would be similar to that which would develop in a repository.

There are no known data in the literature for the mechanical properties of magnetite formed at low temperatures. Most of the available literature data concern magnetite films produced at high temperatures. For example, reference /20/ contains a number of papers that discuss the measurement of mechanical properties of oxide films formed at high temperatures. Some of the key points from papers in reference /20/ are summarised below.

Schutze /21/ showed that:

- the lowest temperature at which creep in the oxide has been observed for magnetite is 600°C,
- the elastic modulus for Fe_3O_4 is 208 GPa,
- KIc 1.4 MPa½ - the paper includes a figure showing the strain to scale failure under tensile stress as a function of defect size,
- Failure strains for oxides on mild steel are typically 1×10^{-4} to 2.3×10^{-4}.

Nagl /22/ measured failure strains at room temperature for iron oxide on mild steel in compression; they varied between –0.13 and –0.5% for oxide thickness between 40 and 6.5 μm. The failure strain also depended on the size of defects present in the oxide, so thinner scales are often more resistant because they have less voidage. Nicholls showed that the elastic modulus of the oxide on mild steel at 550°C was 185 GPa /23/ and the elastic moduli for iron oxides is in the range 151–192 GPa /24/. Microhardness measurements for a magnetite layer on mild steel were 5.5 – 7.6 GPa (peak load over projected contact area). For bulk iron oxide (Fe_3O_4, single crystal), E was 208–210 GPa /25/; this value is similar to the value measured by nano-indentation measurements (Table 2-7). The fracture strain for iron oxide at room temperature depends on the thickness of the iron oxide, ranging from ~0.4% at 5 μm to ~0.1% at 50 μm. This value is higher than those given above by Schutze. The general conclusion is that the magnetite film formed at low temperature under anoxic conditions is considerably more compliant than that formed at high temperature.

3.3 Application of results to assessment of canister performance

If water were to penetrate the outer canister wall and enter the inter-container annulus it is likely that any anaerobic corrosion product formed would deform and spread around the annulus, rather than expand to force the copper outer canister away from the iron insert. Eventually the annulus may fill up with corrosion product, which would gradually be compressed by the

confining walls of the canister. Subsequent corrosion would depend on whether water could penetrate the corrosion product in the annulus and reach the surface of the iron insert. The stress cell experiment did not confine the corrosion products emerging from the interface between the discs and it suggested that future experiments should consider the effect of a more restricted geometry, for example using a defected model canister approach /26/.

Previous work /9,27/ modelled the effect of the accumulation of ferrous corrosion product on the inner container on the expansion of the outer copper canister, assuming certain mechanical properties for the oxide. The present work suggests that the assumptions made in that work were pessimistic in terms of the mechanical properties of the corrosion products, because it was assumed that the oxides would have sufficient mechanical strength to be able to support the applied external load and push the outer copper container away from the cast iron insert. The present work shows that this is unlikely to occur and that the oxide film is compliant rather then being hard. The only remaining question is whether an annulus filled with a compressed oxide could exert a significant expansive force, or whether it would extrude out through the defect.

The lack of any expansion caused by anaerobic corrosion in crevices is supported by the results of a preliminary investigation of natural analogues for expansive corrosion /15,28/, which found that iron-copper archaeological artefacts that had been corroding in anoxic conditions for many centuries did not exhibit any evidence for expansive corrosion.

4 Conclusions

1. A ‘stress cell’ apparatus did not detect any expansion from the anaerobic corrosion of carbon steel or cast iron after more than two years’ exposure to artificial bentonite-equilibrated groundwater under representative applied compressive loads.
2. The anaerobic corrosion product formed on iron-based materials is easily deformed and appears to be incapable of causing expansion of confining metal surfaces under compressive loads that simulate those expected in a repository.
3. Young’s modulus values for anaerobically formed, low temperature magnetite films are in the range 4 × 104 to 2 × 106 Pa, which is several orders of magnitude less than for magnetite films formed at high temperatures.
4. Expansion was observed on a stack of aerobically corroding specimens, but only under very low applied loads.
5. Anaerobic corrosion of polished cast iron in artificial groundwater produces thicker, more compressible layers of friable corrosion product than polished carbon steel.

5 Acknowledgements

The authors are grateful for the financial support provided by SKB and wish to thank Dr. J.A.A. Crossley (Oxford University) for providing the analytical and mechanical properties data, and Mr. P.C. Lovegrove (British Gyroplanes Ltd) for designing and constructing the stress cell apparatus.

6 References

/1/ **J A T Smellie, Wikberg P, 1991.** J. Hydrol 126: p. 129.

/2/ **Smellie J A T, Laaksoharju M, Wikberg P, 1995.** J. Hydrol. 172: p. 147.

/3/ **Brookins DG, 1988.** Eh-pH Diagrams for Geochemistry (Berlin New York: Springer-Verlag).

/4/ **Blackwood D J, Naish C C, Platts N, Taylor K J, Thomas M I, 1995.** The Anaerobic Corrosion of Carbon Steel in Granitic Groundwaters, AEA Technology Report, AEA-InTec-1414.

/5/ **Smart N R, Rance A P, Blackwood D J, 1997.** Corrosion Aspects of the Copper-steel/iron Process Canister: Consequences of Changing the Material for the Inner Container from Carbon Steel to Cast Iron, SKB 97-04, Svensk Kärnbränslehantering AB.

/6/ **Smart N R, Blackwood D J, Werme L, 2001.** The Anaerobic Corrosion of Carbon Steel and Cast Iron in Artificial Groundwaters, SKB TR-01-22, Svensk Kärnbränslehantering AB.

/7/ **Smart N R, Blackwood D J, Werme L, 2002.** Anaerobic Corrosion of Carbon Steel and Cast Iron in Artificial Groundwaters: Part 1–Electrochemical Aspects, Corrosion 58(7), 547.

/8/ **Smart N R, Blackwood D J, Werme L, 2002.** Anaerobic Corrosion of Carbon Steel and Cast Iron in Artificial Groundwaters: Part 2-Gas Generation, Corrosion 58(8), 627.

/9/ **Bond A E, Hoch A R, Jones G D, Tomczyk A J, Wiggin R W, Worraker W J, 1997.** Assessment of a Spent Fuel Disposal Canister. Assessment Studies for a Copper Canister with Cast Steel Inner Component, SKB TR-97-19, Svensk Kärnbränslehantering AB.

/10/ **Pourbaix M, Pourbaix A, Yang X Z, 1981.** Chemical Aspects of Denting in Steam Generators, EPRI report NP-2177.

/11/ **Lloyd G O, Lloyd B, Crouch A G, 1987.** Development of Two Types of Continuous Monitor for Atmospheric Corrosion, U.K. Corrosion'87, p. 403.

/12/ **Manning M I, Crouch A G, Lloyd B, 1988.** A New Method of Monitoring Corrosion, Materials Performance 27(9), 74-78.

/13/ **Lloyd B, 1989.** Real-Time Monitoring of Steel Corrosion Using a Novel Expansion-Based Technique, Paper 22 at Corrosion'89, NACE International, Houston.

/14/ **Smart N R, Bond A E, Crossley J A A, Lovegrove P C, Werme L, 2001.** Mechanical Properties of Oxides Formed by Anaerobic Corrosion of Steel, Materials Research Society Symposium Proceedings Volume 663, Scientific Basis for Nuclear Waste Management XXIV, K.P. Hart and G.R. Lumpkin (eds.), p. 477-485.

/15/ **Smart N R, Rance A P, Fennell P, Werme L, 2003.** Expansion due to Anaerobic Corrosion of Steel and Cast Iron: Experimental and Natural Analogues Studies, in 'Prediction of Long Term Corrosion Behaviour in Nuclear Systems', D. Féron and D.D. Macdonald (eds), European Federation of Corrosion Publications Number 36.

/16/ **Briggs D, Seah MP, Wiley, 1990.** Practical Surface Analysis, 2nd edition, Vol 1.

/17/ **Nicholls J R, Hall D J and Tortorelli P F, 1994.** Hardness and Modulus Measurements on Oxide Scales, Materials at High Temperatures 12(2/3), 141-151.

/18/ **Smart N R, Rance A P and Fennell P A H, 2005.** Galvanic Corrosion of Copper-Cast iron Couples, SA/EIG/13974/C001, 2004 and SKB TR-05-06, Svensk Kärnbränslehantering AB.

/19/ **Smart N R, Fennell P A H, Rance A P and Werme L O, 2004.** Galvanic Corrosion of Copper-Cast Iron Couples in Relation to the Swedish Radioactive Waste Canister Concept, presented at Eurocorr 2005, Nice, September.

/20/ **Special Issue on Mechanical Properties of Protective Oxide Scales, 1994.** Materials at High Temperatures, 12(2/3).

/21/ **Schutze M.** An Approach to a Global Model of the Mechanical Behaviour of Oxide Scales, ibid, p237.

/22/ **Nagl M M, Saunders S R J and Guttmann V.** Experimental Data on Oxide Fracture, ibid, p.163.

/23/ **Nicholls J R, Mendes C and Hancock P.** Measurement Methods to determine the Elastic Properties of oxides at Elevated Temperatures, ibid, p 85.

/24/ **Nicholls J R, Hall D J and Tortorelli P F.** Hardness and Modulus Measurement on Oxide Scales, ibid, p 141.

/25/ **Nagl M M, Evans W T, Hall D J, Saunders S R J, 1994.** An in situ Investigation of the Tensile Failure of Oxide Scales, Oxidation of Metals 42(5/6), 431.

/26/ **Smart N R, Fennell P A H and Knowles G, 2005.** Design of Model Canister Experiments, SA/EIG/11080/C001.

/27/ **SKB, 1999.** Deep repository for Spent Fuel Nuclear Fuel, SR 97 Post closure safety, SKB TR 99 06, Svensk Kärnbränslehantering AB.

/28/ **Smart N R and Adams R, 2005.** Natural Analogues for Expansion due to the Anaerobic Corrosion of Ferrous Materials, SA/EIG/19892/C001.

ISSN 1404-0344
CM Digitaltryck AB, Bromma, 2007